



Published in final edited form as:

J Med Chem. 2013 October 10; 56(19): . doi:10.1021/jm401067s.

Rational development of 4-aminopyridyl-based inhibitors targeting *Trypanosoma cruzi* CYP51 as anti-Chagas agents

Jun Yong Choi¹, Claudia M. Calvet^{2,3,5}, Shamila S. Gunatilleke^{2,3,6}, Claudia Ruiz⁴, Michael D. Cameron⁴, James H. McKerrow^{2,3}, Larissa M. Podust^{2,3,*}, and William R. Roush^{1,*}

¹Department of Chemistry, Scripps Florida, Jupiter, Florida 33458, United States

²Center for Discovery and Innovation in Parasitic Diseases, University of California San Francisco, San Francisco, California 94158, United States

³Department of Pathology, University of California San Francisco, San Francisco, California 94158, United States

⁴Department of Molecular Therapeutics, Scripps Florida, Jupiter, Florida 33458, United States

Abstract

A new series of 4-aminopyridyl-based lead inhibitors targeting *Trypanosoma cruzi* CYP51 (*Tc*CYP51) has been developed using structure-based drug design as well as structure-property relationship (SPR) analyses. The screening hit starting point, LP10 (K_D 42 nM; EC₅₀ of 0.65 μM), has been optimized to give the potential leads **14t**, **27i**, **27q**, **27r**, and **27t**, that have low nanomolar binding affinity to *Tc*CYP51 and significant activity against *T. cruzi* amastigotes cultured in human myoblasts (EC₅₀ = 14–18 nM for **27i** and **27r**). Many of the optimized compounds have improved microsome stability, and most are selective against human CYPs 1A2, 2D6 and 3A4 (<50% inhibition at 1 μM). A rationale for the improvement of microsome stability and selectivity of inhibitors against human metabolic CYP enzymes is presented. In addition, the binding mode of **14t** with the *T. brucei* CYP51 (*Tb*CYP51) ortholog has been characterized by x-ray structure analysis.

Keywords

Chagas disease; non-azole CYP51 inhibitors; structure guided drug design; structure activity and property relationships; x-ray structure

INTRODUCTION

Chagas disease, or American trypanosomiasis is a chronic tropical infection caused by the protozoan parasite *Trypanosoma cruzi*. The infection can be lethal if untreated. Chagas disease is the leading cause of heart failure in Latin America.¹ Although first described a

*To whom correspondence should be addressed. (W.R.R) Tel: (561) 228-2450. Fax: (561) 228-3052. roush@scripps.edu. (L.M.P.) Tel: (415) 514-1381. Fax: (415) 502-8193. larissa.podust@ucsf.edu.

⁵Present Address

Cellular Ultra-Structure Laboratory, Oswaldo Cruz Institute (IOC), FIOCRUZ, Rio de Janeiro, RJ, Brazil 21040-362

⁶College of Science and Engineering, Seattle University, Seattle, Washington 98122, United States

ASSOCIATED CONTENT

Supporting Information. Synthetic procedures and tabulated spectroscopic data for synthetic intermediates. This material is available free of charge via the Internet at <https://pubs.acs.org>.

The atomic coordinates and structure factors (PDB ID code 4BJK) have been deposited in the Protein Data Bank, Research Collaboratory for Structural Bioinformatics, Rutgers University, New Brunswick, NJ (<http://www.rcsb.org/>).

century ago,² it is still a major public health challenge in South America. Furthermore, many cases have been reported in North America, Europe, and Asia due to human population movements, migration of the triatomine insect vectors, HIV-coinfections, and contaminated blood transfusion.^{1b}

Currently nifurtimox and benznidazole are the only drugs approved for treatment of Chagas disease.³ Although these drugs, which date from the late 1960s, show considerable efficacy in the acute stage of Chagas disease, their efficacy is debated in the chronic stage, which involves chronic Chagas cardiomyopathy, leading to congestive heart failure, thromboembolic phenomena, severe arrhythmias, and sudden unexpected death.^{3b, 4} Moreover, these old drugs are associated with frequent side effects such as dermatitis, gastrointestinal, and neurologic toxicities, and even a rare case of bone marrow suppression.^{1a} Therefore, the need exists to develop new therapeutics bearing better safety profiles and improved efficacy to treat *T. cruzi* infections and prevent cardiovascular Chagas disease.

Sterol biosynthesis is a recognized target for the development of new therapeutic agents to treat *T. cruzi* infections.⁵ Sterol 14-demethylase (CYP51) has been successfully targeted for combating pathogenic fungal infections with azole drugs such as fluconazole, ketoconazole, and posaconazole, among others.⁶ CYP51 catalyzes the oxidative removal of the 14-methyl group of lanosterol and produces $\Delta^{14,15}$ -unsaturated intermediates in ergosterol biosynthesis.⁵ Due to the similarity of sterols and their biosynthesis pathways in fungi and *T. cruzi*, the anti-parasitic effects of these azole drugs against *T. cruzi* in infected mammalian cells have been observed.⁷ Therefore, clinical trials of posaconazole and other antifungal agents in combination with benznidazole are underway for treatment of chronic Chagas disease.⁸ Recently, tipifarnib, a class of farnesyl transferase inhibitors, has been repurposed as an anti-parasitic agent in the laboratory setting.⁹ Hit-to-lead optimization of a new "NEU" series, identified via a HTS campaign at Northeastern University, has been achieved (Fig 1).¹⁰ In addition, x-ray co-crystal structures of *T. cruzi* CYP51 (*Tc*CYP51) with bound posaconazole, fluconazole, VNF, and NEU321 have been determined for use in structure-based design approaches to the development of anti-Chagas agents.¹⁰⁻¹¹ However, all of these lead compounds are azoles, and there is an emerging issue of the rapid appearance of laboratory-induced resistance to azoles in *T. cruzi* cell culture.¹² Thus, the development of therapeutics with different scaffolds targeting *Tc*CYP51 is an important undertaking.

Recently, non-azole hits of the LP10 series were identified from a HTS campaign at UC San Francisco.¹³ The binding modes of these non-azole hits were characterized, and their co-crystal structures with *M. tuberculosis* CYP51 (*Mt*CYP51) were determined.^{13a} A 60% cure rate was attained in a mouse model of *T. cruzi* infection using the non-azole CYP51 inhibitor LP10.¹⁴ Accordingly, in an effort to develop more potent non-azole CYP51 inhibitor leads as anti-Chagas agents, we embarked on the optimization of LP10 by using structure-based drug design considerations in conjunction with *in vitro* DMPK analysis (microsome stability and CYP inhibition) to drive rounds of inhibitor optimization. In particular, we strived to increase compound stability in human, rat, and mouse liver microsome preparations, while retaining or increasing inhibition potency toward *T. cruzi* in infected mammalian cells, in order to identify candidates with properties appropriate to advance into animal models of *T. cruzi* infection. In addition, selectivity against human cytochrome P450 enzymes CYP1A2, CYP2C9, CYP2D6, and CYP3A4, the most important CYPs involved in drug metabolism and drug-drug interactions¹⁵, has also been monitored and used for compound prioritization in our structure optimization efforts.

Results and Discussion

Identification of the most active enantiomer of LP10—The original hit (LP10) is a mixture of two racemic diastereomers: S- and R-isomers at the tryptophan unit and cis/trans-isomers within the methylcyclohexane ring. We began by identifying the most active enantiomer of the LP10 scaffold as a starting point for structure optimization. To eliminate the impact of cis/trans isomerization in the methylcyclohexane ring, we evaluated two enantiomerically pure LP10 analogs with a simple cyclohexyl unit (Table 1). The S-isomer **1** has ~30-fold better binding affinity (K_D) toward *T. cruzi* CYP51 than the R-isomer **2**. This result is consistent with the co-crystal structures of LP9 (the methionine analog of LP10) and of LP11 (the valine analog of LP10) with *Mt*CYP51, which have S-enantiomers in the bound structures.^{13a} In addition, the S-isomer **1** had two-fold higher potency (EC50) against *T. cruzi* in infected cells than the R-isomer. Both isomers had similar microsome stability and both were potent inhibitors of human CYP enzymes 2C9, 2D6 and 3A4 (90% inhibition at 10 μ M). Accordingly, we pursued S-enantiomers of LP10 analogs in the development of non-azole CYP51 leads.

Structure activity relationship of initial LP10 analogs—At the outset of these studies, the x-ray structure of *Tc*CYP51 with bound LP10 was not available. Thus, design of initial analog sets was guided by our previous studies on *Mt*CYP51 demonstrating that the hydrophobic contacts experienced by the indole ring accounts for ca. 100-fold increased binding affinity of LP10 toward *Tc*CYP51 ($K_D = 42$ nM), compared to LP9 and LP11 ($K_D = 6,900$ and 9,200 nM, respectively) which have smaller (methylthio)ethyl and isopropyl groups (methionine and valine side chains), respectively.^{13a}

First, we explored the role of the aromatic nitrogen atom in drug-target interactions. Introduction of a methoxy substituent at the 2-position of the 4-acylaminopyridine unit (**3a** in Table 2) resulted in loss of binding affinity toward *Tc*CYP51; **3a** was also inactive against *T. cruzi* in infected cells even at 10 μ M, the highest concentration tested. Similarly, **3b** with a 3,5-dimethylisoxazole unit as a pyridine replacement did not bind to CYP51 and was not active against the parasite in cell-based assays. These results indirectly confirm the binding mode of LP10 that requires coordination of the pyridine nitrogen to the heme iron. Thus, a functional group that hinders the pyridine nitrogen will destabilize the interaction with the heme iron, resulting in a loss of biochemical and cell-based activity. Consistent with this analysis, the ability of **3a** and **3b** to inhibit human CYP enzymes was also significantly decreased compared to LP10.

Second, analogs with secondary or tertiary amine units, such as **3c**, **3d**, **3e**, and **3f**, were also found to have substantially reduced biochemical and cell-based potency, presumably because they are unable to bind in the *Tc*CYP51 active site which accommodates the highly lipophilic natural substrate, lanosterol. However, the microsome stability of **3c**, **3d**, **3e**, and **3f** was significantly increased (30–120 min half-life), and inhibition of human CYP enzymes by these compounds was greatly decreased relative to LP10. Therefore, balancing the charge or polarity distribution of inhibitor analogs was viewed as an important factor to address in the development of more active analogs.

Third, the indole ring of LP10 was replaced with several isosteres. While **3g** and **3i** possessing 3-benzothiophene and N-methyl indole have similar binding affinity to CYP51 as compared to **1** ($K_D = 5$ nM), analogs **3h** and **3j** possessing 1-naphthyl and 5-hydroxy indole units have substantially decreased binding affinity ($K_D = 91$ and 220 nM, respectively). In contrast, introduction of larger hydrophobic substituents at the 5-position of the indole (as in analog **3k**) did not reduce binding affinity to *Tc*CYP51, suggesting that room in the binding site is available to accommodate the bulky substituents at the 5-position of the indole ring

(discussed subsequently in a context of the x-ray structure) without the loss of binding affinity and inhibition potency.

Finally, in order to explore the site of cyclohexane ring binding in *TcCYP51*, the cyclohexanecarboxamide unit was replaced with other aliphatic carboxylamides containing a terminal phenyl ring. We found that analogs **3m** – **3r** have similar binding affinity to *TcCYP51* and comparable inhibition potency against *T. cruzi* in infected cells, compared to those of **1**. However, all of these non-azole inhibitors were rapidly degraded by liver microsome preparations in our standard stability assay using 1 mg/mL hepatic microsomal protein ($t_{1/2} < 6$ min).

Based on the results of this early stage SAR effort (Table 2), plans to increase inhibitor potency of analogs of **1** were formulated and included strategic decisions to: (1) retain the 4-acylamimopyridine moiety as a heme binding unit; (2) retain the indole ring or extend the 5-position of the indole; and, most importantly, (3) to identify replacements for the methylcyclohexane ring to increase microsome stability and decrease inhibition of drug-metabolizing CYP enzymes.

Synthesis of LP10 analogs (1–3r)—Enantiomeric pure **1** was synthesized by the sequence summarized in Scheme 1. Briefly, the *S*-enantiomer of *N*-Boc tryptophan (*L*-tryptophan) was coupled with 4-aminopyridine to produce **5**. Treatment of **5** with 4*N* HCl in dioxane followed by treatment of the deprotected amine with cyclohexanecarbonyl chloride produced enantiomerically pure **1**. A similar sequence, starting from *R*-*N*-Boc tryptophan, was used to synthesize **2** (not shown). Analog **3a** and **3b** were synthesized by replacing 4-aminopyridine with 4-amino-2-methoxypyridine and 4-amino-3,5-dimethylisoxazole, respectively. Acylation of **6** with *N*-Boc-isonipecotic acid followed by treatment with TFA to effect deprotection of the Boc unit provided **3c**, isolated as the HCl salt. Amine salt **3f** was obtained by the alkylation of **6** and benzyl bromide. Various carboxylic acids were coupled with **6** using pentafluorophenyl trifluoroacetate as the dehydrating agent¹⁶ to generate **3d**, **3e**, and **3m** – **3r**. Replacements for the indole moiety of **1** were explored by using commercially available 5-hydroxytryptophan **10** as a starting material. The carboxyl and amine groups were blocked as the methyl ester and *t*-butyl carbamate (Boc), respectively, and **11** was treated with benzyl bromide and Cs₂CO₃ in acetone to produce **12**. Hydrolysis of the methyl ester unit of **12** produced **13**, from which **3k** was obtained by following the procedure for the synthesis of **1**.

Cyclohexyl ring replacement—Based on the initial SAR/SPR analysis, a series of inhibitors were synthesized by using various carboxylic acids to replace the cyclohexylcarboxamide unit of LP10 (Scheme 2 and Table 3). The objective was to increase microsome stability and selectivity against human CYP enzymes, while retaining or increasing inhibition potency against *T. cruzi* in infected cells. First, a benzamide was used to replace the cyclohexylcarboxamide moiety of **1**. The binding affinity ($K_D = 5$ nM), *T. cruzi* inhibition potency ($EC_{50} = 0.39$ nM), microsome stability and inhibition of human CYPs of **14a** were similar to those of **1** (Table 3). The successful replacement of the cyclohexylcarboxamide encouraged us to explore additional substituted benzamide derivatives. Because the phenyl ring of the benzamide is a potential site of metabolism by human CYP enzymes,¹⁷ we anticipated that substitution at the appropriate “soft sites” of the aryl ring could block metabolic oxidation reactions and lead to inhibitors with enhanced microsome stability, while at the same time exploring available space in the active site and hopefully enhancing inhibitor potency against CYP51.

Fluoro, chloro, bromo and other substituents were added to the benzamide unit in attempts to block the potential soft site(s) on the phenyl ring of **14a**. Of the set of inhibitors **14b** –

14k that were synthesized in this effort, several had increased activity against *T. cruzi* in cell culture (**14b**, **14h**, **14j**, **14k**) and while retaining microsomes stability. Acyl groups with larger naphthyl and biaryl units were used in attempts to further improve the microsomes stability (**14l** – **14t**). Gratifyingly, many of these inhibitors had increased microsomes stability, while retaining inhibitor potency. For instance, substitution of a fluorine or a bromine at the 6-position of the naphthyl ring led to **14n** and **14o** with enhanced microsomes stability compared to **1**. Analogs with biaryl units also had enhanced microsomes stability (**14p**, **14r**, **14s**, and **14t**) compared to **1** and **14a**. Of these, analog **14t** was of particular interest as it displayed good inhibition potency ($EC_{50} = 0.19 \mu\text{M}$) against *T. cruzi* in infected cells and moderate (but improved) microsomes stability ($t_{1/2} = 17/25/36 \text{ min}$) against human/rat/mouse liver microsomes.

X-ray structure of 14t complexed with TbCYP51—Although inhibitor design ultimately targeted *TcCYP51*, the best co-crystals with **14t** that diffracted to 2.67 Å were obtained for the *TbCYP51* ortholog (85% sequence identity). The majority of the first tier active site residues are identical between these two parasite CYP51 enzymes, with the exception of substrate-specific F105, which is isoleucine in the *T. cruzi* counterpart. With this difference, the structural information obtained for the *TbCYP51*-**14t** complex facilitated further rounds of structure-based design of *TcCYP51* inhibitors.

Inhibitor **14t** bound in the active site of CYP51 has several interesting features. First, the pyridine nitrogen of the 4-acylaminopyridine unit is coordinated to the heme iron (Fig 2), as expected from the series of the co-structures for the LP10 analogs bound to *MtCYP51*¹⁸. Second, the indole ring of **14t** (PDB small molecule code 18I) occupies the hydrophobic area enclosed largely by the heme macrocycle and the π -electron rich residues Y103, M106, F110, Y116, F290 plus A287 (Fig. 2A); this is the same area where the 2,4-difluorophenyl unit of posaconazole binds (Fig. 2B). Variable F105 is $>5 \text{ \AA}$ away from the indole ring and within 4 Å of the carbonyl group adjacent to the biaryl moiety of **14t**, suggesting additional hydrophobic contacts with the inhibitor in *TbCYP51* which are missing from *T. cruzi* ortholog. Last, the biaryl ring of **14t** projects towards the solvent exposed area, as does the tail part of the posaconazole,¹⁹ but via a different hydrophobic tunnel between the FG-loop (residues 205–210) and the hairpin of the two-stranded β -sheet at the protein C-terminus (residues 459–461) (Fig. 2C).

A hydrophobic cavity accommodating the indole ring of **14t** extends further toward F110 (Fig. 3A) to provide space sufficient to bind a substituted benzyl ring of NEE (PDB ID 4H6O) (Fig. 3B) or a rigid biaryl moiety of VNF (PDB ID 3KSW) (Fig. 3C). In addition to F110, the cavity is enclosed by Y116, providing stacking interactions with the 4-chloro-3,5-dimethylbenzyl unit of NEE, as well as by the aliphatic hydrophobic residues A115, M123, L127, L130, A287, and hydrophilic neutral Q126. Presumably, the bulky substituents at the 5-position of the indole ring in analog **3k** bind in this cavity.

Synthesis of aryl carboxylic acids—The biaryl carboxylic acid intermediates were prepared by palladium-mediated coupling reactions of commercially available 4-bromo-2-fluorobenzoic acid **15** with various aryl boronic acids (Scheme 3). This reaction was performed under microwave irradiation (100 °C for 1 h) and provided products **16** in $>90\%$ yields. Intermediate **17** was obtained by the Heck reaction of **15** and 1-chloro-4-vinylbenzene in the presence of $\text{Pd}(\text{OAc})_2$. Nucleophilic aromatic substitution of **15** with aniline yielded biarylamine **19**. Phenylacetylene was coupled with ester **18** to provide the biaryl acetylene **21a**, which was hydrolyzed under basic conditions to afford **21b**. Treatment of methyl 4-bromo-2-fluorobenzoate (**18**) with morpholine or *N*-Boc-piperazine at 50 °C in toluene gave **22** and **23**; by-products were obtained when this reaction was performed at

higher temperature (ca. 100 °C). The N-Boc protecting group of **23** was removed by treatment with TFA. Aryl sulfonamide **25b** and N-benzylpiperazine **26b** were obtained by the reactions of amine **24** with benzenesulfonyl chloride and benzyl bromide followed by ester hydrolysis under basic conditions, respectively. All benzoic acid derivatives were coupled with indole derivative **6** to generate the inhibitors **27** (Table 4) by using the reaction conditions in Scheme 2.

Structure and property guided optimization of 14t—The terminal phenyl ring of **14t** was extensively modified since it is oriented toward the solvent accessible area and opportunities existed to enhance microsome stability and minimize inhibition of human CYP enzymes through such modifications. Indeed, the substituted biaryl derivatives **27a** – **27n** exhibited enhanced microsome stability, while retaining their inhibition of *T. cruzi* in cell-based assays. It should be noted that all these compounds had low nM affinity for *Tc*CYP51 (Table 4). Of particular interest is that the potency of **27i** in the cell-based *T. cruzi* assay was increased 50-fold ($EC_{50} = 0.014 \mu\text{M}$) compared to that of LP10. Furthermore, **27i** exhibited substantially diminished inhibition of human CYP enzymes (10/91/38/69% inhibition of human CYP1A2/2C9/2D6/3A4 at 1 μM). The microsome stability of analog **27k** significantly increased ($t_{1/2} = 34/125/83$ min, for human, rat and mouse liver microsomes, respectively), and its inhibition of human CYP enzymes was also significantly decreased (% inhibition = 0/85/16/21% at 1 μM), while retaining sub-micromolar potency against *T. cruzi* in infected cells ($EC_{50} = 0.23 \mu\text{M}$).

Lastly, the potency, microsome stability, and CYP selectivity of several aminoaryl-containing analogs was assessed. The morpholinoaryl and sulfonylpiperazine derivatives **27q** and **27r** showed excellent anti-*T. cruzi* potency ($EC_{50} = 0.057$ and $0.018 \mu\text{M}$, respectively), but were moderately stable only in rat liver microsomes ($t_{1/2} = 19$ min). Interestingly, the inhibition potency of amine salt **27s** was slightly improved compared to that of LP10. As discussed previously, the amine salts **3c** – **3f** lost binding affinity and inhibition potency due to the conflict between the polar ammonium ion and the hydrophobic active site of *Tc*CYP51. However, based on the co-crystal structure of **14t** and *Tb*CYP51 (Fig. 3), the polar ammonium ion of **27s** can be oriented toward the solvent accessible area (Fig. 4). The microsome stability of **27s** was also significantly increased, particularly in rat and mouse liver microsomes ($t_{1/2} = 36$ and 41 min respectively), and inhibition of human CYPs was notably decreased. Finally, the inhibition potency of **27t**, which also possesses a basic amine, was ca. 20-fold increased ($EC_{50} = 0.039 \mu\text{M}$) compared to LP10; **27t** was also fairly stable in rat and mouse liver microsomes ($t_{1/2} = 26$ and 20 min, respectively) and exhibited good selectivity toward human CYP enzymes (0/87/51/61% inhibition at 1 μM).

Binding poses of inhibitors 27—All potent inhibitors **27** in Table 4 were docked in the 3D structure of *Tc*CYP51, generated from the x-ray co-crystal structure of *Tb*CYP51 complexed with **14t**, by using Glide XP mode.²⁰ In the results of docking studies, the terminal 3-fluoro-4-hydroxyphenyl ring of **27i** (Fig 4A) and the protonated secondary amine of the piperazine unit of **27s** (Fig 4B) are oriented towards the solvent accessible area. This analysis suggested that unfilled space near the phenolic hydroxyl group of **27i**, could be filled by other substituents, as is the case with O-methyl (in **27i**) and O-benzyl (in **27k**) derivatives. This speculation is consistent with the excellent potency of benzenesulfonamide (**27r**) and benzylamine (**27t**) substituted inhibitors against *T. cruzi*, both of which have relatively large groups that may project into the unfilled region identified above (Fig. 4C, D).

CONCLUSION

The non-azole, indolylpyridinecarboxamide-based CYP51 inhibitor LP10, identified by HTS, was shown in prior studies to have moderate potency ($EC_{50} = 0.65 \mu\text{M}$) against *T. cruzi* in cell culture and to be effective in an acute mouse model of *T. cruzi* infection (60% cure rate).¹⁴ Accordingly, LP10 was selected as the starting point for hit-to-lead optimization, with the objective of improving activity against *T. cruzi* in cell culture, as well as improving microsomal stability and enhancing selectivity against the human CYPs 1A2, 2C9, 2D6 and 3A4. A series of first-generation biaryl inhibitors (e.g., **14t**) were synthesized and shown to have improved microsomal stability and enhanced *in vitro* inhibitor potency (Table 2). The x-ray co-crystal structure of *Tb*CYP51 with bound **14t** was determined and employed in structure-based design of the next round of CYP51 inhibitors. Several potent inhibitors such as **27i**, **27q**, **27r**, and **27t** ($EC_{50} = 14, 57, 18$ and 39 nM against *T. cruzi*) were developed and had the same or better microsomal stability compared to LP10, as well as enhanced selectivity against human CYPs. The microsomal stability of many other inhibitors containing biaryl units, particularly **14t**, **27k**, **27l**, **27p**, and **27s**, was improved, as was the selectivity of **27k** and **27s** when tested against the battery of human CYPs. However, **14t**, **27k**, **27l**, and **27p** were only moderately more potent against *T. cruzi* in cell culture than LP10 ($EC_{50} = 190$ to 470 nM).

Especially noteworthy is that the binding mode of **14t** in the co-crystal structure with *Tb*CYP51 is similar to that of posaconazole with the exception that the biaryl unit of **14t** extends towards the solvent accessible area through a different hydrophobic tunnel than used by posaconazole (Fig. 2B,C). The indole ring of **14t** occupies the same hydrophobic cavity as the 2,4-difluorophenyl moiety of posaconazole. The cavity extends beyond these groups along the heme macrocycle and has sufficient space to accommodate an alkoxy group attached to C5 of the indole nucleus (inhibitor **3k**).

In summary, the SAR/SPR analysis presented here provides a basis to understand the structural features that lead to enhanced biochemical, cell-based activity and microsomal stability of the LP10 series of CYP51 inhibitors. The 4-acylaminopyridine and indole rings of the new inhibitors contribute to their ability to bind tightly to both CYP51 and the human metabolic CYPs in liver microsomes. Introduction of a structurally rigid biaryl unit with appropriately placed substituents resulted in enhanced stability of inhibitors in liver microsomes and also contributed to decreased inhibition of human CYP enzymes, culminating in inhibitor **27k**. In addition, our results show that the binding affinity and inhibition of *Tc*CYP51 as well as other CYP enzymes is highly dependent on the position of amine substituents in the inhibitors due to the hydrophobic nature of the inhibitor binding sites of these enzymes (see data for **3c** – **3f** against **27s** and **27t**). On the other hand, appropriately placed amine substituents contribute to enhanced microsomal stability and diminished inhibition of human CYP enzymes. The design of future generations of CYP51 inhibitors should take these considerations into account.

Experimental Section

Chemistry, General Methods

All reaction solvents were purified before use. Dichloromethane, tetrahydrofuran, dimethylformamide and toluene were purified by passing through a column of activated A-1 alumina. All other reagents purchased from commercial suppliers were used as received. All reactions sensitive to moisture or oxygen were conducted under an argon atmosphere using flame-dried (under vacuum) or oven-dried (overnight) glassware. Removal of solvents was accomplished by using a rotary evaporator under reduced pressure in a water bath below 35

°C, followed by exposure to high vacuum using a vacuum pump. Microwave assisted reactions were performed using a Biotage® Initiator microwave reactor.

Proton nuclear magnetic resonance (^1H NMR) spectra and carbon (^{13}C) NMR spectra were recorded on a commercially available NMR spectrometer at 400 MHz and 100 MHz, respectively. The proton signal for non-deuterated solvent (δ 7.26 for CHCl_3 or δ 2.50 for DMSO) was used as an internal reference for ^1H NMR chemical shifts. Coupling constants (J) are reported in Hertz (Hz). ^{13}C chemical shifts are reported relative to the δ 77.16 resonance of CDCl_3 or the δ 39.52 resonance of DMSO-d_6 .

Analytical thin layer chromatography (TLC) was performed using glass plates precoated with a 0.25-mm thickness of silica gel. The TLC plates were visualized with UV light. Column chromatography was performed using a Biotage® Isolera flash purification system using Biotage® SNAP HP-SIL cartridge (30 μm silica, 10 g to 100 g size). Unless noted otherwise, all compounds isolated by chromatography were sufficiently pure by ^1H NMR analysis for use in subsequent reactions. Polar compounds were purified using preparative high performance liquid chromatography (HPLC) using SunFire column (30 mm \times 250 mm) with a linear gradient elution at 60 mL/min.

The purity of all final compounds (typically 96%) was assayed at 254 nm wavelength by using analytical HPLC (Varian 1100 series) on a reverse phase ZORBAX Eclipse XDB-C18 column (4.6 \times 150 mm, 5 μm). A linear gradient elution ranging from 2% to 98% CH_3CN and H_2O (containing 0.1% TFA and 1% CH_3CN) at 1.5 mL/min was used. Compounds were lyophilized before dissolution in DMSO to give 10 mM stock solutions for use in biochemical and cell-based assays.

Synthesis of inhibitors 1, 2, 3, 14 and 27 by acylation of tryptophan pyridinyl carboxamide (6)

General Procedure A. To a solution of a substituted benzoic or naphthoic acid (ca. 1.2 eq), PyBOP (ca. 1.4 eq) and HOBt (ca. 10 mol%) in dry CH_2Cl_2 (5 mL) was slowly added triethylamine (ca. 4 eq.) at ambient temperature over 15 min. After the reaction mixture became homogenous, **6** was added, and the reaction mixture was stirred at room temperature for 1 h. After completion of the reaction as determined by TLC analysis, the solvent was removed under reduced pressure. The crude mixture was dissolved in ethyl acetate (10 mL) and was washed with saturated aqueous NaHCO_3 (2 mL \times 2) and brine (2 mL \times 2). The organic layer was concentrated in vacuo and directly subjected to purification by flash chromatography to provide the amide products in ca. 80% yield.

(S)-N-(3-(1H-Indol-3-yl)-1-oxo-1-(pyridin-4-ylamino)propan-2-yl)cyclohexanecarboxamide, (1)—To a solution of **6** (0.112 g, 0.353 mmol) in CH_2Cl_2 (10 mL) were added cyclohexanecarbonyl chloride (0.06 mL) and (iPr) $_2$ EtN (0.1 mL) at 0 °C. After 10 min, the reaction mixture was warmed to ambient temperature and stirred for 1 h. After completion of the reaction monitored by TLC, ethyl acetate (40 mL) was added to the crude mixture, which was washed with saturated aqueous NaHCO_3 (10 mL \times 2) and brine (10 mL \times 2). The organic layer was dried over magnesium sulfate, filtered, and concentrated under reduced pressure. Purification of the crude product by flash chromatography provided **1** as a light yellow solid (0.103 g, 0.263 mmol, 75%). ^1H NMR (400 MHz, DMSO-d_6) δ 10.81 (d, J = 2.5 Hz, 1H), 10.56 (s, 1H), 8.50 – 8.38 (m, 2H), 8.06 (d, J = 7.6 Hz, 1H), 7.73 – 7.55 (m, 3H), 7.31 (d, J = 8.1 Hz, 1H), 7.15 (d, J = 2.3 Hz, 1H), 7.04 (ddd, J = 8.1, 7.0, 1.2 Hz, 1H), 7.00 – 6.89 (m, 1H), 4.67 (td, J = 8.4, 5.7 Hz, 1H), 3.22 – 2.94 (m, 2H), 2.19 (ddd, J = 11.1, 7.7, 3.2 Hz, 1H), 1.61 (dt, J = 41.4, 10.3 Hz, 5H), 1.20 (dddd, J = 29.7, 15.4, 12.1, 5.8 Hz, 5H). ^{13}C NMR (101 MHz, DMSO-d_6) δ 175.36, 172.31,

149.72, 146.03, 135.97, 127.19, 123.64, 120.88, 118.50, 118.16, 113.42, 111.24, 109.67, 54.21, 43.45, 29.09, 28.98, 27.58, 25.42, 25.21, 25.16. MS (ESI) 391 m/z [M + H]⁺

(S)-N-(3-(1H-Indol-3-yl)-1-((2-methoxy-pyridin-4-yl)amino)-1-oxopropan-2-yl)cyclohexanecarboxamide (3a)—Compound **3a** was obtained by following the procedure for the synthesis of **1** (69%) as a yellow solid. ¹H NMR (400 MHz, CDCl₃) δ 8.78 (s, 1H), 8.20 (s, 1H), 7.95 (d, J = 5.7 Hz, 1H), 7.64 (d, J = 7.9 Hz, 1H), 7.35 (d, J = 8.1 Hz, 1H), 7.23 – 7.15 (m, 1H), 7.14 – 7.05 (m, 1H), 7.02 (d, J = 2.3 Hz, 1H), 6.89 (d, J = 1.8 Hz, 1H), 6.78 (dd, J = 5.7, 1.9 Hz, 1H), 6.36 (d, J = 7.3 Hz, 1H), 4.93 (q, J = 7.0 Hz, 1H), 3.88 (s, 3H), 3.42 – 3.16 (m, 2H), 2.13 – 2.06 (m, 1H), 1.87 – 1.55 (m, 5H), 1.48 – 1.03 (m, 5H). ¹³C NMR (101 MHz, CDCl₃) δ 177.24, 170.87, 165.37, 147.42, 146.95, 136.35, 127.39, 123.32, 122.63, 120.07, 118.83, 111.49, 110.41, 108.43, 99.77, 54.54, 53.73, 45.26, 29.61, 29.53, 27.76, 25.74, 25.68, 25.63. MS (ESI) 421 m/z [M + H]⁺.

(S)-5-Bromo-N-(1-((3,5-dimethylisoxazol-4-yl)amino)-3-(1H-Indol-3-yl)-1-oxopropan-2-yl)-2-fluorobenzamide (3b)—Compound **3b** (75%) was obtained as a white solid by following the general procedure A with 5-bromo-2-fluorobenzoic acid. ¹H NMR (400 MHz, DMSO-d₆) δ 10.90 (d, J = 2.5 Hz, 1H), 9.48 (s, 1H), 8.71 (dd, J = 7.3, 2.3 Hz, 1H), 7.82 – 7.67 (m, 2H), 7.64 (d, J = 7.9 Hz, 1H), 7.35 (dd, J = 8.1, 0.9 Hz, 1H), 7.29 (dd, J = 10.0, 8.6 Hz, 1H), 7.24 (d, J = 2.4 Hz, 1H), 7.07 (ddd, J = 8.1, 6.9, 1.2 Hz, 1H), 6.98 (ddd, J = 7.9, 6.9, 1.0 Hz, 1H), 4.80 (td, J = 7.8, 6.5 Hz, 1H), 3.39 – 3.09 (m, 2H), 2.12 (s, 3H), 1.95 (s, 3H). ¹³C NMR (101 MHz, DMSO-d₆) δ 170.77, 162.42, 162.36, 159.74, 157.49, 157.25, 136.09, 135.13, 132.41, 132.38, 127.26, 125.69, 125.53, 123.89, 120.97, 118.77, 118.53, 118.44, 118.31, 115.91, 115.88, 113.94, 111.34, 109.48, 54.59, 27.43, 10.57, 9.22. MS (ESI) 499/501 m/z [M + H]⁺.

(S)-N-(3-(1H-Indol-3-yl)-1-oxo-1-(pyridin-4-ylamino)propan-2-yl)piperidine-4-carboxamide hydrochloride (3c)—To a solution of **9** (0.12 g, 0.25 mmol) in CH₂Cl₂ (10 mL) was added trifluoroacetic acid (0.5 mL), and the reaction mixture was stirred for 1 h at room temperature. After removing solvent under reduced pressure, the reaction mixture was directly subjected to HPLC, and the product **3c** (58 mg, 0.15 mmol, 47%) was obtained as a white solid. ¹H NMR (400 MHz, DMSO-d₆) δ 11.44 (s, 1H), 10.90 (d, J = 2.5 Hz, 1H), 8.80 (s, 1H), 8.68 – 8.61 (m, 2H), 8.49 (d, J = 7.3 Hz, 1H), 8.00 – 7.93 (m, 2H), 7.63 (d, J = 7.8 Hz, 1H), 7.36 – 7.23 (m, 2H), 7.21 (d, J = 1.9 Hz, 2H), 7.18 – 6.91 (m, 3H), 4.72 (ddd, J = 9.0, 7.3, 5.5 Hz, 1H), 3.30 – 3.15 (m, 2H), 3.09 (dd, J = 14.6, 9.0 Hz, 1H), 2.95 – 2.73 (m, 2H), 1.85 (dd, J = 14.4, 3.8 Hz, 1H), 1.79 – 1.51 (m, 3H). ¹³C NMR (101 MHz, DMSO-d₆) δ 173.41, 173.12, 158.33, 158.02, 151.00, 144.33, 136.02, 127.09, 123.92, 120.95, 118.24, 115.59, 114.26, 111.33, 109.20, 54.90, 42.28, 38.28, 27.28, 24.98. MS (ESI) 392.4 m/z [M + H]⁺.

(S)-N-(3-(1H-Indol-3-yl)-1-oxo-1-(pyridin-4-ylamino)propan-2-yl)-1-methylpiperidine-4-carboxamide (3d)—Compound **3d** (47%) as a yellow solid was obtained by following the procedure for the synthesis of **9** with 1-methylpiperidine-4-carboxylic acid. ¹H NMR (400 MHz, DMSO-d₆) δ 11.31 (s, 1H), 10.93 (d, J = 2.5 Hz, 1H), 8.67 – 8.44 (m, 3H), 7.84 (d, J = 6.0 Hz, 2H), 7.66 (d, J = 7.9 Hz, 1H), 7.31 (d, J = 8.0 Hz, 1H), 7.21 (d, J = 2.3 Hz, 1H), 7.08 – 6.99 (m, 1H), 6.94 (t, J = 7.3 Hz, 1H), 4.72 (q, J = 7.5 Hz, 1H), 3.44 – 3.27 (m, 2H), 3.27 – 3.02 (m, 2H), 2.99 – 2.76 (m, 2H), 2.66 (s, 3H), 2.04 – 1.57 (m, 5H). ¹³C NMR (101 MHz, DMSO-d₆) δ 173.03, 172.60, 148.52, 147.02, 139.68, 136.01, 127.21, 123.87, 120.91, 118.57, 118.22, 113.87, 111.32, 109.45, 108.75, 54.91, 52.45, 42.47, 38.41, 27.54, 25.67. MS (ESI) 406 m/z [M + H]⁺.

N-((S)-3-(1H-Indol-3-yl)-1-oxo-1-(pyridin-4-ylamino)propan-2-yl)-1-methylpiperidine-3-carboxamide (3e)—Compound **3e** (light yellow, racemic mixture) was obtained by following the procedure for the synthesis of **9** with 1-methylpiperidine-3-carboxylic acid (58%). ¹H NMR (400 MHz, DMSO-d₆) δ 11.57 (d, J = 6.3 Hz, 1H), 10.95 (dd, J = 14.9, 2.5 Hz, 1H), 8.75 (dd, J = 19.9, 7.4 Hz, 1H), 8.61 (dd, J = 6.1, 3.7 Hz, 2H), 7.96 (d, J = 5.9 Hz, 2H), 7.67 (d, J = 7.9 Hz, 1H), 7.45 (s, 1H), 7.37 – 7.28 (m, 2H), 7.27 – 7.16 (m, 2H), 7.11 – 6.99 (m, 1H), 6.95 (dd, J = 7.6, 4.8 Hz, 1H), 4.73 (t, J = 7.5 Hz, 1H), 3.40 – 2.72 (m, 6H), 2.67 (d, J = 4.2 Hz, 3H), 2.05 – 1.68 (m, 3H). ¹³C NMR (101 MHz, DMSO-d₆) δ 172.71, 158.41, 158.11, 150.31, 145.03, 136.03, 136.00, 127.15, 124.02, 120.91, 118.69, 118.57, 118.28, 115.71, 114.18, 114.12, 111.35, 109.26, 109.20, 55.10, 53.74, 52.86, 42.79, 27.24, 25.46, 22.52, 21.87. MS (ESI) 406 *m/z* [M + H]⁺.

(S)-2-((2-Fluorobenzyl)amino)-3-(1H-indol-3-yl)-N-(pyridin-4-yl)propanamide hydrochloride (3f)—To a solution of **6** (0.107 g, 0.338 mmol) in CH₂Cl₂ were added Et₃N (0.05 mL) and 2-fluorobenzylbromide (0.06 mL), and the reaction mixture was stirred at room temperature for 12 h. Solvent was removed by using rotary evaporator, and the product mixture was directly subjected to HPLC. The product **3f** (38.7 mg, 0.0997 mmol, 30%) was obtained as a white solid. ¹H NMR (400 MHz, DMSO-d₆) δ 10.86 (d, J = 2.5 Hz, 1H), 8.94 (d, J = 8.3 Hz, 1H), 8.26 (dd, J = 7.5, 1.8 Hz, 1H), 8.12 (dd, J = 7.3, 1.9 Hz, 1H), 7.90 – 7.77 (m, 1H), 7.63 (d, J = 7.7 Hz, 1H), 7.51 – 7.42 (m, 1H), 7.42 – 7.21 (m, 6H), 7.18 (d, J = 2.4 Hz, 1H), 7.08 – 6.92 (m, 3H), 6.73 (dd, J = 7.6, 2.9 Hz, 1H), 5.39 (s, 2H), 4.51 (td, J = 8.6, 5.1 Hz, 1H), 3.44 – 2.98 (m, 2H). ¹³C NMR (101 MHz, DMSO-d₆) δ 171.66, 158.96, 156.65, 143.80, 141.67, 136.00, 131.30, 130.44, 130.41, 127.04, 125.12, 125.08, 124.07, 122.52, 120.95, 118.37, 115.92, 115.72, 111.32, 111.11, 109.13, 105.57, 56.65, 54.15, 28.01. MS (ESI) 389 *m/z* [M + H]⁺.

(S)-N-(3-(Benzo[b]thiophen-3-yl)-1-oxo-1-(pyridin-4-ylamino)propan-2-yl)cyclohexanecarboxamide (3g)—Compound **3g** (68%) was obtained as a white solid by following the procedure for the synthesis of **1** with Boc-L-3-benzothierylalanine. ¹H NMR (400 MHz, DMSO-d₆) δ 10.58 (s, 1H), 8.54 – 8.37 (m, 2H), 8.23 (d, J = 7.9 Hz, 1H), 8.05 – 7.90 (m, 2H), 7.67 – 7.54 (m, 2H), 7.45 (s, 1H), 7.44 – 7.33 (m, 2H), 4.81 (ddd, J = 9.5, 7.9, 5.1 Hz, 1H), 3.46 – 3.05 (m, 2H), 2.17 (ddd, J = 10.9, 7.5, 3.5 Hz, 1H), 1.77 – 1.44 (m, 6H), 1.36 – 1.01 (m, 4H). ¹³C NMR (101 MHz, DMSO-d₆) δ 175.44, 171.62, 150.29, 145.48, 139.47, 138.62, 131.74, 124.27, 123.96, 123.89, 122.81, 121.99, 113.43, 52.91, 43.50, 30.44, 29.12, 28.89, 25.41, 25.22, 25.13. MS (ESI) 408.2 *m/z* [M + H]⁺.

(S)-N-(3-(Naphthalen-1-yl)-1-oxo-1-(pyridin-4-ylamino)propan-2-yl)cyclohexanecarboxamide (3h)—Compound **3h** (67%) was obtained as a white solid by following the procedure for the synthesis of **1** with Boc-L-1-naphthylalanine. ¹H NMR (400 MHz, DMSO-d₆) δ 10.47 (s, 1H), 8.49 – 8.37 (m, 2H), 8.24 (t, J = 8.0 Hz, 2H), 7.91 (dd, J = 7.9, 1.4 Hz, 1H), 7.78 (dd, J = 7.5, 1.9 Hz, 1H), 7.64 – 7.46 (m, 4H), 7.46 – 7.32 (m, 2H), 4.82 (td, J = 8.5, 5.8 Hz, 1H), 3.61 – 3.26 (m, 2H), 2.16 (dtd, J = 15.7, 8.4, 7.6, 4.1 Hz, 1H), 1.73 – 1.41 (m, 5H), 1.36 – 0.95 (m, 5H). ¹³C NMR (101 MHz, DMSO-d₆) δ 175.39, 171.60, 150.31, 145.38, 133.33, 133.24, 131.67, 128.51, 127.29, 127.13, 126.07, 125.57, 125.22, 123.92, 113.48, 53.85, 43.47, 34.49, 29.14, 28.87, 25.41, 25.22, 25.12. MS (ESI) 402.3 *m/z* [M + H]⁺.

(S)-N-(3-(1-Methyl-1H-Indol-3-yl)-1-oxo-1-(pyridin-4-ylamino)propan-2-yl)cyclohexanecarboxamide (3i)—Compound **3i** (51%) was obtained as a yellow solid by following the procedures for the synthesis of **13** and **1** starting with 1-methyl-L-tryptophan. R_f = 0.57 (10% MeOH in ethyl acetate). ¹H NMR (400 MHz, DMSO-d₆) δ 10.46 (s, 1H), 8.51 – 8.33 (m, 2H), 8.04 (d, J = 7.8 Hz, 1H), 7.64 (d, J = 7.9 Hz, 1H), 7.60 –

7.51 (m, 2H), 7.35 (d, $J = 8.2$ Hz, 1H), 7.17 – 7.07 (m, 2H), 6.99 (t, $J = 7.4$ Hz, 1H), 4.66 (td, $J = 8.2, 5.6$ Hz, 1H), 3.70 (s, 3H), 3.21 – 2.95 (m, 2H), 2.29 – 2.14 (m, 1H), 1.77 – 1.49 (m, 5H), 1.40 – 1.01 (m, 5H). ^{13}C NMR (101 MHz, DMSO- d_6) δ 175.37, 172.06, 150.30, 145.48, 136.45, 128.04, 127.53, 121.02, 118.80, 118.26, 113.35, 109.45, 109.13, 54.24, 43.45, 32.26, 29.05, 29.00, 27.50, 25.42, 25.20, 25.15. MS (ESI) 405 m/z $[\text{M} + \text{H}]^+$.

(S)-N-(3-(5-Hydroxy-1H-Indol-3-yl)-1-oxo-1-(pyridin-4-ylamino)propan-2-yl)cyclohexanecarboxamide (3j)—To a solution of **3k** (0.328 g, 0.66 mmol) in methanol (10 mL) was added 10% Pd/C (ca. 30 mg) at room temperature. After air was removed from the flask using a vacuum pump, hydrogen gas was introduced using a balloon. The reaction mixture was stirred for 1h, and the flask was evacuated under vacuum and refilled with hydrogen gas. This procedure was repeated three times, and the reaction mixture was stirred overnight at ambient temperature. Palladium on carbon was removed by filtration through Celite pad. The filtrate was collected and evaporated to give the crude product, which was purified by flash chromatography to afford the product **3j** as a brown solid (0.077 g, 0.19 mmol, 29%). ^1H NMR (400 MHz, DMSO- d_6) δ 10.47 (d, $J = 3.6$ Hz, 1H), 8.55 (s, 1H), 8.48 – 8.33 (m, 2H), 8.01 (d, $J = 7.7$ Hz, 1H), 7.66 – 7.49 (m, 2H), 7.09 (d, $J = 8.5$ Hz, 1H), 7.04 (d, $J = 2.4$ Hz, 1H), 6.93 (d, $J = 2.2$ Hz, 1H), 6.58 (dd, $J = 8.6, 2.3$ Hz, 1H), 4.63 (td, $J = 8.2, 6.0$ Hz, 1H), 3.15 – 2.83 (m, 2H), 2.19 (ddd, $J = 14.4, 9.5, 3.5$ Hz, 1H), 1.91 (s, 1H), 1.63 (dd, $J = 32.3, 11.3$ Hz, 5H), 1.38 – 1.00 (m, 5H). ^{13}C NMR (101 MHz, DMSO- d_6) δ 175.33, 172.27, 150.30, 150.20, 145.50, 130.54, 127.96, 123.98, 113.36, 111.46, 111.24, 108.72, 102.55, 54.02, 43.46, 29.13, 28.99, 27.67, 25.43, 25.23, 25.17, 21.07. MS (ESI) 407 m/z $[\text{M} + \text{H}]^+$.

(S)-N-(3-(5-(Benzyloxy)-1H-Indol-3-yl)-1-oxo-1-(pyridin-4-ylamino)propan-2-yl)cyclohexanecarboxamide (3k)—The procedure for the synthesis of **1** was followed using **13** to provide **3k** as a light yellow solid (52%, over 3 steps). $R_f = 0.21$ (100% ethyl acetate), $R_f = 0.63$ (10% MeOH in ethyl acetate). ^1H NMR (400 MHz, DMSO- d_6) δ 10.67 (d, $J = 2.6$ Hz, 1H), 10.52 (s, 1H), 8.41 (d, $J = 5.5$ Hz, 2H), 8.08 (d, $J = 7.8$ Hz, 1H), 7.58 (d, $J = 5.5$ Hz, 2H), 7.46 (d, $J = 7.5$ Hz, 2H), 7.39 (t, $J = 7.5$ Hz, 2H), 7.32 (t, $J = 7.2$ Hz, 1H), 7.24 (d, $J = 2.2$ Hz, 1H), 7.21 (d, $J = 8.7$ Hz, 1H), 7.12 (d, $J = 2.3$ Hz, 1H), 6.77 (dd, $J = 8.6, 2.3$ Hz, 1H), 5.16 – 4.90 (m, 2H), 4.66 (td, $J = 8.3, 5.4$ Hz, 1H), 3.17 – 2.90 (m, 2H), 2.27 – 2.13 (m, 1H), 1.61 (dt, $J = 32.1, 11.7$ Hz, 5H), 1.36 – 1.00 (m, 5H). ^{13}C NMR (101 MHz, DMSO- d_6) δ 175.32, 172.24, 152.06, 150.32, 145.51, 137.78, 131.34, 128.33, 127.65, 127.60, 124.45, 113.34, 111.80, 111.40, 109.58, 102.22, 69.90, 54.28, 43.51, 29.08, 29.00, 27.73, 25.43, 25.22, 25.18. MS (ESI) 497 m/z $[\text{M} + \text{H}]^+$.

(S)-N-(3-(1H-Indol-3-yl)-1-oxo-1-(pyridin-4-ylamino)propan-2-yl)-4,4-difluorocyclohexanecarboxamide (3l)—The procedure for the synthesis of **9** was followed using 4,4-difluorocyclohexanecarboxylic acid to provide **3l** as a light yellow solid (41%). $R_f = 0.39$ (100% ethyl acetate), ^1H NMR (400 MHz, DMSO- d_6) δ 10.81 (d, $J = 2.4$ Hz, 1H), 10.51 (s, 1H), 8.52 – 8.37 (m, 2H), 8.23 (d, $J = 7.8$ Hz, 1H), 7.63 (d, $J = 7.8$ Hz, 1H), 7.60 – 7.52 (m, 2H), 7.31 (dt, $J = 8.1, 0.9$ Hz, 1H), 7.15 (d, $J = 2.3$ Hz, 1H), 7.05 (ddd, $J = 8.1, 7.0, 1.2$ Hz, 1H), 6.96 (ddd, $J = 8.0, 6.9, 1.1$ Hz, 1H), 4.71 (td, $J = 8.4, 5.5$ Hz, 1H), 3.24 – 2.94 (m, 2H), 2.42 – 2.29 (m, 1H), 2.07 – 1.37 (m, 8H). ^{13}C NMR (101 MHz, DMSO- d_6) δ 173.93, 172.03, 150.33, 145.46, 135.99, 127.19, 123.65, 120.91, 118.52, 118.17, 113.36, 111.25, 109.63, 54.19, 40.44, 30.67, 27.65, 25.52, 25.43, 25.38, 25.29. MS (ESI) 427.1 m/z $[\text{M} + \text{H}]^+$.

(S)-3-(1H-Indol-3-yl)-2-(2-phenylacetamido)-N-(pyridin-4-yl)propanamide (3m)—The procedure for the synthesis of **1** was followed using 2-phenylacetyl chloride to provide **3m** as a yellow solid (61%). $R_f = 0.30$ (100% ethyl acetate). ^1H NMR (400 MHz,

DMSO- d_6) δ 10.94 – 10.73 (m, 1H), 10.54 (s, 1H), 8.50 (d, J = 7.6 Hz, 1H), 8.46 – 8.31 (m, 2H), 7.63 (d, J = 7.9 Hz, 1H), 7.59 – 7.49 (m, 2H), 7.32 (d, J = 8.1 Hz, 1H), 7.29 – 7.09 (m, 6H), 7.05 (t, J = 7.5 Hz, 1H), 6.95 (t, J = 7.4 Hz, 1H), 4.72 (td, J = 8.3, 5.6 Hz, 1H), 3.46 (d, J = 2.2 Hz, 2H), 3.25 – 2.97 (m, 2H). ^{13}C NMR (101 MHz, DMSO- d_6) δ 171.93, 170.16, 150.33, 145.42, 136.20, 136.02, 128.96, 128.08, 127.17, 126.21, 123.74, 120.90, 118.51, 118.22, 113.37, 111.26, 109.47, 68.24, 54.48, 41.85. MS (ESI) 399 m/z $[\text{M} + \text{H}]^+$.

(S)-3-(1H-Indol-3-yl)-2-(3-phenylpropanamido)-N-(pyridin-4-yl)propanamide

(3n)—The procedure for the synthesis of **9** was followed using 3-phenylpropanoic acid to provide **3n** as a yellow solid (73%). R_f = 0.33 (100% ethyl acetate). ^1H NMR (400 MHz, DMSO- d_6) δ 10.81 (d, J = 2.5 Hz, 1H), 10.50 (s, 1H), 8.50 – 8.37 (m, 2H), 8.30 (d, J = 7.7 Hz, 1H), 7.63 (d, J = 7.9 Hz, 1H), 7.60 – 7.54 (m, 2H), 7.35 – 7.28 (m, 1H), 7.25 – 7.09 (m, 6H), 7.06 (ddd, J = 8.1, 6.9, 1.2 Hz, 1H), 6.97 (ddd, J = 8.0, 6.9, 1.1 Hz, 1H), 4.72 (td, J = 8.2, 5.9 Hz, 1H), 3.25 – 2.92 (m, 2H), 2.74 (dd, J = 8.7, 6.8 Hz, 2H), 2.42 (dd, J = 8.8, 6.7 Hz, 2H). ^{13}C NMR (101 MHz, DMSO- d_6) δ 172.01, 171.53, 150.31, 145.46, 141.20, 136.02, 128.19, 128.14, 127.19, 125.79, 123.64, 120.91, 118.50, 118.21, 113.37, 111.27, 109.62, 54.38, 36.68, 30.96, 27.66. MS (ESI) 413 m/z $[\text{M} + \text{H}]^+$.

(S)-N-(3-(1H-Indol-3-yl)-1-oxo-1-(pyridin-4-ylamino)propan-2-yl)-4-phenylbutanamide (3o)

—The procedure for the synthesis of **9** was followed using 4-phenylbutanoic acid to provide **3o** as a yellow solid (67%). R_f = 0.33 (100% ethyl acetate). ^1H NMR (400 MHz, CDCl_3) δ 9.28 (s, 1H), 8.37 – 8.26 (m, 2H), 7.57 (dd, J = 8.0, 1.0 Hz, 1H), 7.38 – 7.34 (m, 2H), 7.32 (dt, J = 8.1, 1.0 Hz, 1H), 7.26 (s, 3H), 7.20 – 7.14 (m, 2H), 7.09 – 7.04 (m, 2H), 7.04 – 7.00 (m, 2H), 6.42 (d, J = 7.3 Hz, 1H), 4.96 (q, J = 7.1 Hz, 1H), 3.29 (dd, J = 7.0, 1.9 Hz, 2H), 2.54 (t, J = 7.6 Hz, 2H), 2.18 (td, J = 7.4, 2.0 Hz, 2H), 1.87 (p, J = 7.9 Hz, 2H). ^{13}C NMR (101 MHz, CDCl_3) δ 174.04, 171.16, 149.27, 145.96, 141.20, 136.36, 128.60, 128.53, 127.32, 126.26, 123.40, 122.64, 120.09, 118.58, 114.05, 111.62, 110.09, 54.97, 35.73, 35.09, 27.78, 27.01. MS (ESI) 427 m/z $[\text{M} + \text{H}]^+$.

(S)-3-(1H-Indol-3-yl)-2-(3-(4-methoxyphenyl)propanamido)-N-(pyridin-4-yl)propanamide (3p)

—The procedure for the synthesis of **9** was followed using 3-(4-methoxyphenyl)propanoic acid to provide **3p** as a yellow solid (34%). ^1H NMR (400 MHz, CDCl_3) δ 8.98 (s, 1H), 8.42 – 8.33 (m, 2H), 8.33 – 8.24 (m, 1H), 7.55 (d, J = 7.8 Hz, 1H), 7.38 – 7.32 (m, 1H), 7.32 – 7.27 (m, 2H), 7.18 (ddd, J = 8.2, 7.0, 1.1 Hz, 1H), 7.07 (ddd, J = 8.1, 7.0, 1.0 Hz, 1H), 7.02 – 6.94 (m, 2H), 6.90 (d, J = 2.4 Hz, 1H), 6.75 – 6.70 (m, 2H), 6.40 (d, J = 7.4 Hz, 1H), 4.90 (q, J = 7.0 Hz, 1H), 3.71 (s, 3H), 3.34 – 3.12 (m, 2H), 2.88 – 2.74 (m, 2H), 2.46 (t, J = 7.7 Hz, 2H). ^{13}C NMR (101 MHz, CDCl_3) δ 173.49, 170.91, 158.26, 149.75, 145.45, 136.33, 132.29, 129.35, 127.36, 123.40, 122.62, 120.08, 118.57, 114.14, 114.01, 111.59, 110.04, 55.38, 54.84, 38.40, 30.65, 27.40. MS (ESI) 443 m/z $[\text{M} + \text{H}]^+$.

(S)-3-(1H-Indol-3-yl)-N-(pyridin-4-yl)-2-(3-(4-

(trifluoromethyl)phenyl)propanamido)-propanamide (3q)—The procedure for the synthesis of **9** was followed using 3-(4-(trifluoromethyl)phenyl)propanoic acid to provide **3q** as a yellow solid (17%). ^1H NMR (400 MHz, CDCl_3) δ 8.71 (s, 1H), 8.41 – 8.34 (m, 2H), 8.29 (s, 1H), 7.59 (d, J = 7.8 Hz, 1H), 7.44 (d, J = 8.1 Hz, 2H), 7.36 (dt, J = 8.2, 0.9 Hz, 1H), 7.29 – 7.16 (m, 5H), 7.09 (ddd, J = 8.0, 7.0, 1.0 Hz, 1H), 6.97 (d, J = 2.4 Hz, 1H), 6.44 (d, J = 7.3 Hz, 1H), 4.90 (q, J = 7.2 Hz, 1H), 3.42 – 3.13 (m, 2H), 2.94 (t, J = 7.5 Hz, 2H), 2.51 (td, J = 7.5, 2.7 Hz, 2H). ^{13}C NMR (101 MHz, CDCl_3) δ 172.70, 170.71, 149.97, 145.17, 144.48, 136.38, 128.74, 127.26, 125.66, 125.62, 125.58, 123.41, 122.77, 120.22, 118.55, 113.93, 111.68, 110.03, 54.90, 37.53, 31.13, 27.62. MS (ESI) 481 m/z $[\text{M} + \text{H}]^+$.

(S)-N-(3-(1H-Indol-3-yl)-1-oxo-1-(pyridin-4-ylamino)propan-2-yl)-4-(4-fluorophenyl)butanamide (3r)—The procedure for the synthesis of **9** was followed using 4-(4-fluorophenyl)butanoic acid to provide **3r** as a solid (86%). $R_f = 0.24$ (100% ethyl acetate). $^1\text{H NMR}$ (400 MHz, DMSO-d_6) δ 10.91 – 10.76 (m, 1H), 10.54 (s, 1H), 8.53 – 8.37 (m, 2H), 8.23 (d, $J = 7.7$ Hz, 1H), 7.65 (d, $J = 7.8$ Hz, 1H), 7.61 – 7.56 (m, 2H), 7.31 (d, $J = 8.0$ Hz, 1H), 7.17 (d, $J = 2.3$ Hz, 1H), 7.15 – 7.00 (m, 5H), 6.96 (t, $J = 7.4$ Hz, 1H), 4.73 (td, $J = 8.5, 5.7$ Hz, 1H), 3.23 – 2.93 (m, 2H), 2.44 (t, $J = 7.6$ Hz, 2H), 2.23 – 2.01 (m, 2H), 1.70 (p, $J = 7.4$ Hz, 2H). $^{13}\text{C NMR}$ (101 MHz, DMSO-d_6) δ 172.22, 172.05, 161.75, 159.35, 150.07, 145.72, 137.85, 137.82, 136.02, 130.01, 129.93, 127.17, 123.66, 120.91, 118.53, 118.19, 114.93, 114.72, 113.39, 111.27, 109.67, 54.36, 34.30, 33.54, 27.60, 26.99. MS (ESI) 445 m/z $[\text{M} + \text{H}]^+$.

(S)-tert-Butyl (3-(1H-Indol-3-yl)-1-oxo-1-(pyridin-4-ylamino)propan-2-yl)carbamate, (5)—To a solution of N-Boc-L-tryptophan (1.0 g, 3.3 mmol), PyBOP (2.0 g, 3.9 mmol), and HOBt (0.29 g) in dry CH_2Cl_2 (20 mL) was slowly added triethylamine (1.5 mL, ca. 4 eq.) at 0 °C, and the reaction mixture was stirred and warmed to ambient temperature for 15 min. After the mixture was cooled to 0 °C, 4-aminopyridine (0.39 g, 4.1 mmol) was added, and the reaction mixture was stirred at room temperature for 1 h. After completion of the reaction monitored by TLC, ethyl acetate (80 mL) was added to the crude mixture, which was washed with saturated aqueous NaHCO_3 (20 mL \times 2) and brine (20 mL \times 2). The organic layer was dried over magnesium sulfate, filtered, and concentrated in vacuo. Purification of the crude product by flash chromatography provided 0.98 g (94%) of **5** as a light yellow solid. $R_f = 0.45$ (100% ethyl acetate). $^1\text{H NMR}$ (400 MHz, CDCl_3) δ 9.07 (s, 1H), 8.86 (dd, $J = 23.3, 11.0$ Hz, 1H), 8.36 – 8.23 (m, 2H), 7.58 (d, $J = 8.0$ Hz, 1H), 7.31 (d, $J = 8.3$ Hz, 1H), 7.23 (d, $J = 5.7$ Hz, 2H), 7.14 (t, $J = 7.7$ Hz, 1H), 7.03 (t, $J = 7.6$ Hz, 1H), 6.98 (s, 1H), 5.57 (q, $J = 7.5, 6.2$ Hz, 1H), 4.67 (s, 1H), 3.40 – 3.15 (m, 2H), 1.39 (s, 9H). $^{13}\text{C NMR}$ (101 MHz, CDCl_3) δ 171.75, 156.25, 150.26, 145.03, 136.47, 127.27, 123.51, 122.34, 119.79, 118.62, 113.90, 111.52, 109.94, 80.82, 56.04, 28.37, 22.61. MS (ESI) 381 m/z $[\text{M} + \text{H}]^+$.

(S)-N-(3-(1H-Indol-3-yl)-1-oxo-1-(pyridin-4-ylamino)propan-2-yl)benzamide (14a)—The procedure for the synthesis of **1** was followed using benzoyl chloride to provide **14a** as a solid (99%). $R_f = 0.39$ (100% ethyl acetate). $^1\text{H NMR}$ (400 MHz, DMSO-d_6) δ 10.82 (d, $J = 2.5$ Hz, 1H), 10.64 (s, 1H), 8.74 (d, $J = 7.5$ Hz, 1H), 8.56 – 8.37 (m, 2H), 7.92 – 7.80 (m, 2H), 7.75 (d, $J = 7.7$ Hz, 1H), 7.67 – 7.61 (m, 2H), 7.58 – 7.39 (m, 3H), 7.32 (d, $J = 8.1$ Hz, 1H), 7.28 (d, $J = 2.3$ Hz, 1H), 7.06 (ddd, $J = 8.1, 6.9, 1.2$ Hz, 1H), 6.99 (ddd, $J = 8.1, 6.9, 1.1$ Hz, 1H), 4.89 (ddd, $J = 9.1, 7.5, 5.6$ Hz, 1H), 3.41 – 3.15 (m, 2H). $^{13}\text{C NMR}$ (101 MHz, DMSO-d_6) δ 172.19, 166.50, 150.33, 145.55, 136.03, 133.75, 131.42, 128.19, 127.50, 127.15, 123.87, 120.95, 118.60, 118.22, 113.41, 111.32, 109.95, 55.28, 27.24. MS (ESI) 385 m/z $[\text{M} + \text{H}]^+$.

(S)-N-(3-(1H-Indol-3-yl)-1-oxo-1-(pyridin-4-ylamino)propan-2-yl)-2-fluorobenzamide (14b)—The procedure for the synthesis of **1** was followed using 2-fluorobenzoyl chloride to provide **14b** as a light yellow solid (49%). $R_f = 0.18$ (100% ethyl acetate). $^1\text{H NMR}$ (400 MHz, DMSO-d_6) δ 10.87 (d, $J = 2.5$ Hz, 1H), 10.63 (s, 1H), 8.50 (dd, $J = 7.3, 3.6$ Hz, 1H), 8.47 – 8.29 (m, 2H), 7.66 (d, $J = 7.8$ Hz, 1H), 7.60 (qd, $J = 5.3, 1.8$ Hz, 3H), 7.57 – 7.49 (m, 1H), 7.33 (d, $J = 8.1$ Hz, 1H), 7.31 – 7.21 (m, 3H), 7.06 (ddd, $J = 8.0, 6.9, 1.2$ Hz, 1H), 6.96 (ddd, $J = 7.9, 6.9, 1.1$ Hz, 1H), 4.89 (td, $J = 8.1, 5.5$ Hz, 1H), 3.40 – 3.11 (m, 2H). $^{13}\text{C NMR}$ (101 MHz, DMSO-d_6) δ 171.52, 163.60, 160.61, 158.13, 150.37, 145.46, 136.06, 132.77, 130.33, 130.30, 127.17, 124.45, 124.41, 123.93, 123.09, 122.95, 120.97, 118.48, 118.25, 116.24, 116.02, 113.43, 111.33, 109.35, 55.08, 27.41. MS (ESI) 403 m/z $[\text{M} + \text{H}]^+$.

(S)-N-(3-(1H-Indol-3-yl)-1-oxo-1-(pyridin-4-ylamino)propan-2-yl)-3-fluorobenzamide (14c)—The procedure for the synthesis of **1** was followed using 3-fluorobenzoyl chloride to provide **14c** as a yellow solid (51%). $R_f = 0.21$ (100% ethyl acetate). $^1\text{H NMR}$ (400 MHz, DMSO- d_6) δ 10.82 (d, $J = 2.5$ Hz, 1H), 10.66 (s, 1H), 8.88 (d, $J = 7.5$ Hz, 1H), 8.44 (d, $J = 5.6$ Hz, 2H), 7.74 (d, $J = 7.8$ Hz, 1H), 7.71 (dt, $J = 7.7, 1.2$ Hz, 1H), 7.69–7.63 (m, 1H), 7.63–7.59 (m, 2H), 7.51 (td, $J = 8.0, 5.8$ Hz, 1H), 7.38 (td, $J = 8.3, 2.7$ Hz, 1H), 7.31 (d, $J = 8.0$ Hz, 1H), 7.27 (d, $J = 2.4$ Hz, 1H), 7.06 (ddd, $J = 8.1, 6.9, 1.2$ Hz, 1H), 7.02–6.94 (m, 1H), 4.89 (ddd, $J = 9.4, 7.5, 5.4$ Hz, 1H), 3.45–3.16 (m, 2H). $^{13}\text{C NMR}$ (101 MHz, DMSO- d_6) δ 171.99, 165.18, 163.07, 150.26, 145.60, 136.03, 130.45, 127.13, 123.86, 123.72, 120.97, 118.59, 118.24, 113.45, 111.33, 109.86, 55.38, 27.22. MS (ESI) 403.2 m/z $[\text{M} + \text{H}]^+$.

(S)-N-(3-(1H-Indol-3-yl)-1-oxo-1-(pyridin-4-ylamino)propan-2-yl)-3-phenoxybenzamide (14d)—The procedure for the synthesis of **9** was followed using 3-phenoxybenzoic acid to provide **14d** as a white solid (84%). $R_f = 0.60$ (10% MeOH in ethyl acetate). $^1\text{H NMR}$ (400 MHz, DMSO- d_6) δ 10.80 (d, $J = 2.5$ Hz, 1H), 10.63 (s, 1H), 8.82 (d, $J = 7.6$ Hz, 1H), 8.55–8.40 (m, 2H), 7.73 (d, $J = 7.8$ Hz, 1H), 7.65 (dt, $J = 7.8, 1.2$ Hz, 1H), 7.63–7.57 (m, 2H), 7.53–7.36 (m, 4H), 7.31 (d, $J = 8.1$ Hz, 1H), 7.24 (d, $J = 2.4$ Hz, 1H), 7.21–7.13 (m, 2H), 7.09–7.00 (m, 3H), 7.00–6.92 (m, 1H), 4.86 (ddd, $J = 9.3, 7.5, 5.5$ Hz, 1H), 3.32–3.11 (m, 2H). $^{13}\text{C NMR}$ (101 MHz, DMSO- d_6) δ 172.06, 165.66, 156.62, 156.39, 150.31, 145.54, 136.01, 135.63, 130.15, 129.98, 127.12, 123.85, 123.73, 122.54, 121.68, 120.94, 118.73, 118.59, 118.22, 117.57, 113.42, 111.31, 109.91, 55.34, 27.18. MS (ESI) 477 m/z $[\text{M} + \text{H}]^+$.

(S)-N-(3-(1H-Indol-3-yl)-1-oxo-1-(pyridin-4-ylamino)propan-2-yl)-4-(trifluoromethyl)benzamide (14e)—The procedure for the synthesis of **1** was followed using 4-trifluoromethylbenzoyl chloride to provide **14e** as a white solid (50%). $R_f = 0.27$ (100% ethyl acetate). $^1\text{H NMR}$ (400 MHz, DMSO- d_6) δ 10.81 (d, $J = 2.5$ Hz, 1H), 10.66 (s, 1H), 9.04 (d, $J = 7.5$ Hz, 1H), 8.58–8.27 (m, 2H), 8.05 (d, $J = 8.1$ Hz, 2H), 7.84 (d, $J = 8.3$ Hz, 2H), 7.74 (d, $J = 7.6$ Hz, 1H), 7.66–7.56 (m, 2H), 7.38–7.28 (m, 1H), 7.26 (d, $J = 2.3$ Hz, 1H), 7.06 (ddd, $J = 8.2, 7.0, 1.3$ Hz, 1H), 6.99 (ddd, $J = 7.9, 6.8, 1.1$ Hz, 1H), 4.92 (ddd, $J = 9.3, 7.5, 5.4$ Hz, 1H), 3.39–3.15 (m, 2H). $^{13}\text{C NMR}$ (101 MHz, DMSO- d_6) δ 171.87, 165.37, 150.36, 145.48, 137.51, 136.03, 128.43, 127.14, 125.26, 123.82, 120.97, 118.58, 118.24, 113.44, 111.32, 109.84, 55.39, +27.25. MS (ESI) 453.3 m/z $[\text{M} + \text{H}]^+$.

(S)-N-(3-(1H-Indol-3-yl)-1-oxo-1-(pyridin-4-ylamino)propan-2-yl)-4-methoxybenzamide (14f)—The procedure for the synthesis of **1** was followed using 4-methoxybenzoyl chloride to provide **14f** as a yellow solid (90%). $^1\text{H NMR}$ (400 MHz, DMSO- d_6) δ 10.81 (d, $J = 2.5$ Hz, 1H), 10.62 (s, 1H), 8.58 (d, $J = 7.6$ Hz, 1H), 8.47–8.37 (m, 2H), 7.90–7.81 (m, 2H), 7.74 (d, $J = 7.8$ Hz, 1H), 7.66–7.58 (m, 2H), 7.31 (dt, $J = 8.1, 1.0$ Hz, 1H), 7.26 (d, $J = 2.4$ Hz, 1H), 7.14–6.88 (m, 4H), 4.86 (ddd, $J = 9.1, 7.5, 5.7$ Hz, 1H), 3.80 (d, $J = 2.8$ Hz, 3H), 3.39–3.18 (m, 2H). $^{13}\text{C NMR}$ (101 MHz, DMSO- d_6) δ 172.39, 165.96, 161.71, 150.34, 145.57, 136.02, 129.38, 127.16, 125.94, 123.85, 120.93, 118.61, 118.22, 113.39, 111.31, 110.02, 55.34, 55.25, 27.24. MS (ESI) 415 m/z $[\text{M} + \text{H}]^+$.

(S)-N-(3-(1H-Indol-3-yl)-1-oxo-1-(pyridin-4-ylamino)propan-2-yl)-2-chlorobenzamide (14g)—The procedure for the synthesis of **1** was followed using 2-chlorobenzoyl chloride to provide **14g** as a yellow solid (83%). $R_f = 0.54$ (10% MeOH in ethyl acetate). $^1\text{H NMR}$ (400 MHz, DMSO- d_6) δ 10.95–10.79 (m, 1H), 10.59 (s, 1H), 8.85 (d, $J = 7.6$ Hz, 1H), 8.50–8.35 (m, 2H), 7.68 (d, $J = 7.9$ Hz, 1H), 7.62–7.56 (m, 2H), 7.50–7.40 (m, 2H), 7.40–7.28 (m, 3H), 7.24 (d, $J = 2.3$ Hz, 1H), 7.11–7.03 (m, 1H), 6.98 (t, $J = 7.5$ Hz, 1H), 4.90 (td, $J = 8.5, 5.9$ Hz, 1H), 3.42–3.08 (m, 2H). $^{13}\text{C NMR}$ (101 MHz,

DMSO- d_6) δ 171.53, 166.33, 150.35, 145.49, 136.16, 136.04, 130.90, 130.06, 129.59, 129.09, 127.19, 126.89, 123.84, 120.93, 118.53, 118.21, 113.40, 111.28, 109.57, 54.85, 27.39. MS (ESI) 419 m/z [M + H]⁺.

(S)-N-(3-(1H-Indol-3-yl)-1-oxo-1-(pyridin-4-ylamino)propan-2-yl)-2,5-difluorobenzamide (14h)—The procedure for the synthesis of **1** was followed using 2,5-difluorobenzoyl chloride to provide **14h** as a light yellow solid (50%). R_f = 0.39 (100% ethyl acetate). ¹H NMR (400 MHz, DMSO- d_6) δ 12.31 (s, 1H), 11.00 (d, J = 2.5 Hz, 1H), 8.83 (dd, J = 7.0, 2.8 Hz, 1H), 8.72 (d, J = 7.0 Hz, 2H), 8.31 – 8.15 (m, 2H), 7.72 (d, J = 7.8 Hz, 1H), 7.47 – 7.27 (m, 5H), 7.10 – 6.98 (m, 1H), 6.93 (t, J = 7.4 Hz, 1H), 4.96 (ddd, J = 8.9, 7.0, 5.4 Hz, 1H), 3.50 – 3.18 (m, 2H). ¹³C NMR (101 MHz, DMSO- d_6) δ 172.85, 162.66, 158.86, 156.79, 156.46, 154.35, 152.93, 142.15, 136.07, 127.15, 124.34, 124.27, 124.18, 124.11, 120.98, 119.60, 119.51, 119.36, 119.27, 118.58, 118.30, 118.23, 118.06, 117.98, 116.53, 116.50, 116.28, 116.25, 114.62, 114.56, 111.38, 108.94, 55.95, 26.99. MS (ESI) 421 m/z [M + H]⁺.

(S)-N-(3-(1H-Indol-3-yl)-1-oxo-1-(pyridin-4-ylamino)propan-2-yl)-2,4-difluorobenzamide (14i)—The procedure for the synthesis of **1** was followed using 2,4-difluorobenzoyl chloride to provide **14i** as a light yellow solid (68%). R_f = 0.39 (100% ethyl acetate). ¹H NMR (400 MHz, DMSO- d_6) δ 10.93 – 10.83 (m, 1H), 10.65 (s, 1H), 8.54 (dd, J = 7.4, 3.2 Hz, 1H), 8.49 – 8.39 (m, 2H), 7.66 (dd, J = 8.3, 6.9 Hz, 2H), 7.63 – 7.55 (m, 2H), 7.34 (t, J = 8.6 Hz, 2H), 7.24 (d, J = 2.3 Hz, 1H), 7.17 (td, J = 8.5, 2.4 Hz, 1H), 7.06 (t, J = 7.5 Hz, 1H), 6.97 (t, J = 7.4 Hz, 1H), 4.88 (td, J = 8.2, 5.7 Hz, 1H), 3.53 – 3.08 (m, 2H). ¹³C NMR (101 MHz, DMSO- d_6) δ 171.48, 162.83, 162.22, 150.37, 145.45, 136.05, 131.99, 127.15, 123.92, 120.97, 119.77, 119.73, 118.47, 118.25, 113.43, 111.65, 111.33, 109.33, 104.59, 55.13, 27.40. MS (ESI) 421 m/z [M + H]⁺.

(S)-N-(3-(1H-Indol-3-yl)-1-oxo-1-(pyridin-4-ylamino)propan-2-yl)-5-bromo-2-fluorobenzamide (14j)—The general procedure A was followed using 5-bromo-2-fluorobenzoic acid to provide **14j** as a light yellow solid (67%). ¹H NMR (400 MHz, DMSO- d_6) δ 10.87 (d, J = 2.4 Hz, 1H), 10.63 (s, 1H), 8.74 (dd, J = 7.5, 2.3 Hz, 1H), 8.51 – 8.37 (m, 2H), 7.72 (ddd, J = 8.7, 4.4, 2.6 Hz, 1H), 7.69 – 7.63 (m, 2H), 7.62 – 7.56 (m, 2H), 7.33 (d, J = 8.1 Hz, 1H), 7.28 (dd, J = 10.0, 8.8 Hz, 1H), 7.22 (d, J = 2.4 Hz, 1H), 7.10 – 7.02 (m, 1H), 6.97 (t, J = 7.5 Hz, 1H), 4.88 (td, J = 8.3, 5.6 Hz, 1H), 3.39 – 3.07 (m, 2H). ¹³C NMR (101 MHz, DMSO- d_6) δ 171.33, 162.38, 150.37, 145.41, 136.03, 132.41, 127.17, 123.85, 120.98, 118.55, 118.48, 118.26, 115.94, 113.44, 111.33, 109.37, 55.16, 27.40. MS (ESI) 481/483 m/z [M + H]⁺.

(S)-N-(3-(1H-Indol-3-yl)-1-oxo-1-(pyridin-4-ylamino)propan-2-yl)-4-bromo-2-fluorobenzamide (14k)—The general procedure A was followed using 4-bromo-2-fluorobenzoic acid to provide **14k** as a yellow solid (70%). R_f = 0.30 (100% ethyl acetate). ¹H NMR (400 MHz, DMSO- d_6) δ 10.86 (d, J = 2.3 Hz, 1H), 10.67 (s, 1H), 8.62 (dd, J = 7.4, 2.8 Hz, 1H), 8.51 – 8.36 (m, 2H), 7.70 – 7.63 (m, 2H), 7.63 – 7.58 (m, 2H), 7.51 (d, J = 6.4 Hz, 2H), 7.33 (d, J = 8.0 Hz, 1H), 7.22 (d, J = 2.3 Hz, 1H), 7.06 (t, J = 7.6 Hz, 1H), 6.96 (t, J = 7.4 Hz, 1H), 4.88 (td, J = 8.2, 5.6 Hz, 1H), 3.50 – 3.04 (m, 2H). ¹³C NMR (101 MHz, DMSO- d_6) δ 171.44, 162.92, 157.93, 150.14, 145.64, 136.04, 131.77, 127.70, 127.14, 123.90, 120.97, 119.41, 118.47, 118.25, 113.46, 111.33, 109.29, 55.14, 27.39. MS (ESI) 481/483 m/z [M + H]⁺.

(S)-N-(3-(1H-Indol-3-yl)-1-oxo-1-(pyridin-4-ylamino)propan-2-yl)-2-naphthamide (14l)—The general procedure A was followed using 2-naphthoic acid to provide **14l** as a yellow solid (24%). R_f = 0.30 (100% ethyl acetate). ¹H NMR (400 MHz, DMSO- d_6) δ 10.83

(s, 1H), 10.67 (s, 1H), 8.91 (d, $J = 7.5$ Hz, 1H), 8.48 (s, 1H), 8.44 (d, $J = 5.4$ Hz, 2H), 8.12 – 7.87 (m, 4H), 7.78 (d, $J = 7.8$ Hz, 1H), 7.70 – 7.52 (m, 4H), 7.32 (d, $J = 7.9$ Hz, 2H), 7.03 (dt, $J = 23.4, 7.2$ Hz, 2H), 4.96 (q, $J = 7.5$ Hz, 1H), 3.44 – 3.21 (m, 2H). ^{13}C NMR (101 MHz, DMSO- d_6) δ 172.15, 166.52, 150.35, 145.54, 136.04, 134.20, 132.03, 131.08, 128.82, 127.88, 127.77, 127.69, 127.61, 127.22, 126.74, 124.31, 123.86, 120.96, 118.63, 118.25, 113.43, 111.33, 109.98, 55.42, 27.33. MS (ESI) 435 m/z $[\text{M} + \text{H}]^+$.

(S)-N-(3-(1H-Indol-3-yl)-1-oxo-1-(pyridin-4-ylamino)propan-2-yl)-1-fluoro-2-naphthamide (14m)—The procedure for the synthesis of **1** was followed using 1-fluoro-2-naphthoic acid to provide **14m** as a yellow solid (61%). ^1H NMR (400 MHz, DMSO- d_6) δ 10.97 – 10.83 (m, 1H), 10.67 (s, 1H), 8.67 (dd, $J = 7.5, 3.5$ Hz, 1H), 8.51 – 8.42 (m, 2H), 8.23 – 8.08 (m, 1H), 8.08 – 7.98 (m, 1H), 7.82 (d, $J = 8.5$ Hz, 1H), 7.75 – 7.56 (m, 6H), 7.34 (d, $J = 8.0$ Hz, 1H), 7.27 (d, $J = 2.3$ Hz, 1H), 7.06 (t, $J = 7.5$ Hz, 1H), 6.96 (t, $J = 7.4$ Hz, 1H), 4.97 (td, $J = 8.0, 5.6$ Hz, 1H), 3.48 – 3.15 (m, 2H). ^{13}C NMR (101 MHz, DMSO- d_6) δ 171.51, 163.76, 150.31, 145.52, 136.06, 135.32, 128.53, 127.68, 127.45, 127.22, 125.52, 123.89, 123.76, 122.60, 122.43, 120.97, 118.49, 118.26, 113.45, 111.33, 109.39, 55.21, 27.49. MS (ESI) 453 m/z $[\text{M} + \text{H}]^+$.

(S)-N-(3-(1H-Indol-3-yl)-1-oxo-1-(pyridin-4-ylamino)propan-2-yl)-6-fluoro-2-naphthamide (14n)—The general procedure A was followed using 6-fluoro-2-naphthoic acid to provide **14n** as a light yellow solid (42%). $R_f = 0.27$ (100% ethyl acetate). ^1H NMR (400 MHz, DMSO- d_6) δ 10.83 (d, $J = 2.5$ Hz, 1H), 10.67 (s, 1H), 8.91 (d, $J = 7.6$ Hz, 1H), 8.52 (d, $J = 1.2$ Hz, 1H), 8.48 – 8.38 (m, 2H), 8.10 (dd, $J = 9.1, 5.8$ Hz, 1H), 7.97 (d, $J = 1.2$ Hz, 2H), 7.84 – 7.73 (m, 2H), 7.69 – 7.60 (m, 2H), 7.51 (td, $J = 8.9, 2.6$ Hz, 1H), 7.40 – 7.26 (m, 2H), 7.06 (ddd, $J = 8.2, 7.0, 1.3$ Hz, 1H), 7.03 – 6.95 (m, 1H), 4.96 (ddd, $J = 9.1, 7.5, 5.6$ Hz, 1H), 3.44 – 3.18 (m, 2H). ^{13}C NMR (101 MHz, DMSO- d_6) δ 172.12, 166.33, 159.74, 150.31, 145.58, 136.04, 135.22, 135.13, 131.96, 131.86, 130.65, 129.23, 128.01, 127.31, 127.21, 125.40, 123.85, 120.96, 118.62, 118.26, 116.89, 113.44, 111.34, 109.95, 55.41, 27.35. MS (ESI) 453 m/z $[\text{M} + \text{H}]^+$.

(S)-N-(3-(1H-Indol-3-yl)-1-oxo-1-(pyridin-4-ylamino)propan-2-yl)-6-bromo-2-naphthamide (14o)—The general procedure A was followed using 6-bromo-2-naphthoic acid to provide **14o** as a light yellow solid (76%). $R_f = 0.36$ (100% ethyl acetate). ^1H NMR (400 MHz, DMSO- d_6) δ 10.92 – 10.74 (m, 2H), 8.98 (d, $J = 7.5$ Hz, 1H), 8.57 – 8.41 (m, 3H), 8.28 (d, $J = 2.0$ Hz, 1H), 7.98 (d, $J = 6.1$ Hz, 3H), 7.85 – 7.63 (m, 4H), 7.32 (d, $J = 7.8$ Hz, 2H), 7.03 (dt, $J = 24.7, 7.2$ Hz, 2H), 4.96 (td, $J = 8.4, 5.7$ Hz, 1H), 3.32 (qd, $J = 14.6, 7.3$ Hz, 2H). ^{13}C NMR (101 MHz, DMSO- d_6) δ 172.23, 166.27, 149.45, 146.35, 136.03, 135.29, 131.63, 131.03, 130.58, 129.80, 129.59, 127.95, 127.19, 127.07, 125.49, 123.88, 121.07, 120.96, 118.60, 118.25, 113.56, 111.34, 109.88, 55.54, 27.29. MS (ESI) 515 m/z $[\text{M} + \text{H}]^+$.

(S)-N-(3-(1H-Indol-3-yl)-1-oxo-1-(pyridin-4-ylamino)propan-2-yl)-[1,1'-biphenyl]-4-carboxamide (14p)—The general procedure A was followed using [1,1'-biphenyl]-4-carboxylic acid to provide **14p** as a light yellow solid (28%). $R_f = 0.36$ (100% ethyl acetate). ^1H NMR (400 MHz, DMSO- d_6) δ 10.83 (d, $J = 2.5$ Hz, 1H), 10.66 (s, 1H), 8.81 (d, $J = 7.6$ Hz, 1H), 8.51 – 8.39 (m, 2H), 7.96 (d, $J = 8.4$ Hz, 2H), 7.81 – 7.70 (m, 5H), 7.67 – 7.60 (m, 2H), 7.56 – 7.45 (m, 2H), 7.44 – 7.37 (m, 1H), 7.32 (d, $J = 8.1$ Hz, 1H), 7.29 (d, $J = 2.3$ Hz, 1H), 7.11 – 7.03 (m, 1H), 7.00 (t, $J = 7.4$ Hz, 1H), 4.92 (td, $J = 8.1, 7.7, 5.8$ Hz, 1H), 3.45 – 3.21 (m, 2H). ^{13}C NMR (101 MHz, DMSO- d_6) δ 172.21, 166.15, 150.36, 145.56, 142.92, 139.10, 136.04, 132.54, 129.02, 128.21, 128.07, 127.17, 126.86, 126.40, 123.86, 120.95, 118.61, 118.24, 113.42, 111.32, 109.98, 55.32, 27.25. MS (ESI) 461 m/z $[\text{M} + \text{H}]^+$.

(S)-N-(3-(1H-Indol-3-yl)-1-oxo-1-(pyridin-4-ylamino)propan-2-yl)-[1,1'-biphenyl]-3-carboxamide (14q)—The general procedure A was followed using [1,1'-biphenyl]-3-carboxylic acid to provide **14q** as a yellow solid (42%). $R_f = 0.30$ (100% ethyl acetate). $^1\text{H NMR}$ (400 MHz, DMSO- d_6) δ 10.90 – 10.80 (m, 1H), 10.66 (s, 1H), 8.94 (d, $J = 7.7$ Hz, 1H), 8.50 – 8.37 (m, 2H), 8.14 (d, $J = 1.8$ Hz, 1H), 7.83 (dd, $J = 7.8, 1.8$ Hz, 2H), 7.78 (d, $J = 7.8$ Hz, 1H), 7.76 – 7.71 (m, 2H), 7.66 – 7.61 (m, 2H), 7.53 (dt, $J = 11.7, 7.7$ Hz, 3H), 7.41 (t, $J = 7.3$ Hz, 1H), 7.35 – 7.26 (m, 2H), 7.05 (t, $J = 7.5$ Hz, 1H), 6.99 (t, $J = 7.4$ Hz, 1H), 5.01 – 4.88 (m, 1H), 3.42 – 3.17 (m, 2H). $^{13}\text{C NMR}$ (101 MHz, DMSO- d_6) δ 172.15, 166.41, 150.36, 145.53, 140.07, 139.47, 136.01, 134.42, 129.59, 128.98, 128.95, 127.78, 127.22, 126.84, 126.73, 125.65, 123.81, 120.94, 118.62, 118.25, 113.42, 111.32, 110.03, 55.44, 27.30. MS (ESI) 461 m/z $[\text{M} + \text{H}]^+$.

(S)-N-(3-(1H-Indol-3-yl)-1-oxo-1-(pyridin-4-ylamino)propan-2-yl)-2-fluoro-[1,1'-biphenyl]-4-carboxamide (14r)—The general procedure A was followed using 3-fluoro-[1,1'-biphenyl]-4-carboxylic acid to provide **14r** as a light yellow solid (78%). $R_f = 0.36$ (100% ethyl acetate). $^1\text{H NMR}$ (400 MHz, DMSO- d_6) δ 10.83 (d, $J = 2.5$ Hz, 1H), 10.66 (s, 1H), 8.93 (d, $J = 7.6$ Hz, 1H), 8.60 – 8.35 (m, 2H), 7.91 – 7.71 (m, 3H), 7.70 – 7.56 (m, 5H), 7.55 – 7.40 (m, 3H), 7.32 (d, $J = 7.9$ Hz, 1H), 7.28 (d, $J = 2.3$ Hz, 1H), 7.10 – 7.03 (m, 1H), 7.00 (t, $J = 7.5$ Hz, 1H), 4.92 (ddd, $J = 9.3, 7.4, 5.4$ Hz, 1H), 3.33 (s, 2H). $^{13}\text{C NMR}$ (101 MHz, DMSO- d_6) δ 171.99, 164.88, 159.88, 157.44, 150.36, 145.53, 136.04, 134.24, 131.02, 130.71, 128.85, 128.83, 128.71, 128.40, 127.15, 124.04, 123.86, 120.98, 118.60, 118.26, 113.46, 111.35, 109.89, 55.38, 27.25. MS (ESI) 479 m/z $[\text{M} + \text{H}]^+$.

(S)-N-(3-(1H-Indol-3-yl)-1-oxo-1-(pyridin-4-ylamino)propan-2-yl)-3-fluoro-[1,1'-biphenyl]-4-carboxamide (14s)—The general procedure A was followed using **16s** to provide **14s** as a yellow solid (37%). $^1\text{H NMR}$ (400 MHz, DMSO- d_6) δ 10.88 (d, $J = 2.7$ Hz, 1H), 10.64 (s, 1H), 8.58 – 8.37 (m, 3H), 7.79 – 7.57 (m, 8H), 7.54 – 7.46 (m, 2H), 7.47 – 7.40 (m, 1H), 7.36 – 7.31 (m, 1H), 7.25 (d, $J = 2.4$ Hz, 1H), 7.06 (ddd, $J = 8.1, 6.9, 1.2$ Hz, 1H), 6.96 (ddd, $J = 8.1, 6.9, 1.0$ Hz, 1H), 4.91 (td, $J = 7.9, 5.5$ Hz, 1H), 3.32 (s, 2H). $^{13}\text{C NMR}$ (101 MHz, DMSO- d_6) δ 171.49, 150.35, 145.44, 137.75, 136.05, 129.07, 127.16, 126.90, 123.91, 121.49, 121.35, 120.95, 118.46, 118.25, 113.92, 113.42, 109.31, 55.08, 27.42. MS (ESI) 479 m/z $[\text{M} + \text{H}]^+$.

(S)-N-(3-(1H-Indol-3-yl)-1-oxo-1-(pyridin-4-ylamino)propan-2-yl)-3,3'-difluoro-[1,1'-biphenyl]-4-carboxamide (14t)—The general procedure A was followed using **16t** to provide **14t** as a light yellow solid (54%). $R_f = 0.45$ (100% ethyl acetate). $^1\text{H NMR}$ (400 MHz, DMSO- d_6) δ 10.88 (d, $J = 2.4$ Hz, 1H), 10.65 (s, 1H), 8.53 (dd, $J = 7.4, 3.8$ Hz, 1H), 8.45 (d, $J = 5.6$ Hz, 2H), 7.88 – 7.58 (m, 8H), 7.58 – 7.47 (m, 1H), 7.33 (d, $J = 8.1$ Hz, 1H), 7.31 – 7.19 (m, 2H), 7.06 (t, $J = 7.5$ Hz, 1H), 6.97 (t, $J = 7.5$ Hz, 1H), 4.97 – 4.84 (m, 1H), 3.46 – 3.17 (m, 2H). $^{13}\text{C NMR}$ (101 MHz, DMSO) δ 171.49, 163.89, 163.22, 161.47, 161.08, 158.60, 150.37, 145.46, 136.07, 131.09, 131.00, 127.18, 123.92, 123.03, 122.61, 122.17, 122.03, 120.98, 118.48, 118.26, 113.87, 113.65, 113.43, 111.34, 109.34, 55.11, 27.43. MS (ESI) 497 m/z $[\text{M} + \text{H}]^+$.

(S)-N-(3-(1H-Indol-3-yl)-1-oxo-1-(pyridin-4-ylamino)propan-2-yl)-3,4'-difluoro-[1,1'-biphenyl]-4-carboxamide (27a)—The general procedure A was followed using **16a** to provide **27a** as a light yellow solid (64%). $R_f = 0.42$ (100% ethyl acetate). $^1\text{H NMR}$ (400 MHz, DMSO- d_6) δ 10.88 (d, $J = 2.6$ Hz, 1H), 10.67 (s, 1H), 8.54 – 8.39 (m, 3H), 7.88 – 7.76 (m, 2H), 7.74 – 7.55 (m, 6H), 7.33 (ddd, $J = 8.8, 6.7, 2.2$ Hz, 3H), 7.25 (d, $J = 2.4$ Hz, 1H), 7.06 (ddd, $J = 8.1, 6.9, 1.2$ Hz, 1H), 7.01 – 6.88 (m, 1H), 4.91 (td, $J = 8.1, 5.6$ Hz, 1H), 3.45 – 3.17 (m, 2H). $^{13}\text{C NMR}$ (101 MHz, DMSO- d_6) δ 171.53, 163.25, 161.28, 161.12, 158.64, 150.21, 145.61, 143.65, 143.57, 136.07, 130.98, 129.15, 129.06, 127.18, 123.92,

122.42, 120.98, 118.47, 118.26, 116.03, 115.82, 113.94, 113.46, 111.34, 109.32, 55.12, 27.42. MS (ESI) 497 m/z [M + H]⁺.

(S)-N-(3-(1H-Indol-3-yl)-1-oxo-1-(pyridin-4-ylamino)propan-2-yl)-2',3-difluoro-[1,1'-biphenyl]-4-carboxamide (27b)—The general procedure A was followed using **16b** to provide **27b** as a light yellow solid (74%). ¹H NMR (400 MHz, DMSO-*d*₆) δ 10.88 (d, *J* = 2.5 Hz, 1H), 10.67 (s, 1H), 8.58 (dd, *J* = 7.3, 3.5 Hz, 1H), 8.53 – 8.36 (m, 2H), 7.73 – 7.64 (m, 2H), 7.64 – 7.57 (m, 3H), 7.48 (ddt, *J* = 9.7, 6.4, 1.4 Hz, 3H), 7.40 – 7.30 (m, 3H), 7.25 (d, *J* = 2.3 Hz, 1H), 7.06 (ddd, *J* = 8.1, 6.9, 1.2 Hz, 1H), 6.97 (ddd, *J* = 7.9, 6.9, 1.0 Hz, 1H), 4.91 (td, *J* = 8.2, 5.6 Hz, 1H), 3.44 – 3.15 (m, 2H). ¹³C NMR (101 MHz, DMSO-*d*₆) δ 171.53, 163.31, 160.49, 160.24, 157.79, 150.14, 145.68, 139.51, 136.07, 130.75, 130.49, 127.17, 125.14, 125.10, 123.94, 122.30, 122.16, 120.98, 118.48, 118.26, 116.40, 116.18, 113.49, 111.34, 109.33, 55.14, 27.41. MS (ESI) 497 m/z [M + H]⁺.

(S)-N-(3-(1H-Indol-3-yl)-1-oxo-1-(pyridin-4-ylamino)propan-2-yl)-3,3',5'-trifluoro-[1,1'-biphenyl]-4-carboxamide (27c)—The general procedure A was followed using **16c** to provide **27c** as a light yellow solid (73%). *R*_f = 0.30 (100% ethyl acetate). ¹H NMR (400 MHz, DMSO-*d*₆) δ 10.88 (d, *J* = 2.5 Hz, 1H), 10.65 (s, 1H), 8.57 (dd, *J* = 7.4, 3.6 Hz, 1H), 8.51 – 8.34 (m, 2H), 7.83 – 7.72 (m, 1H), 7.73 – 7.64 (m, 3H), 7.63 – 7.55 (m, 4H), 7.37 – 7.27 (m, 2H), 7.25 (d, *J* = 2.3 Hz, 1H), 7.06 (ddd, *J* = 8.1, 6.9, 1.2 Hz, 1H), 7.01 – 6.93 (m, 1H), 4.91 (td, *J* = 8.2, 5.6 Hz, 1H), 3.40 – 3.16 (m, 2H). ¹³C NMR (101 MHz, DMSO-*d*₆) δ 171.48, 164.17, 164.03, 163.18, 161.72, 161.59, 161.01, 150.37, 145.46, 136.07, 130.93, 127.18, 123.92, 122.81, 122.72, 122.68, 120.99, 118.49, 118.27, 116.00, 114.71, 114.48, 113.45, 111.34, 110.37, 110.11, 109.34, 55.13, 27.43. MS (ESI) 515 m/z [M + H]⁺.

(S)-N-(3-(1H-Indol-3-yl)-1-oxo-1-(pyridin-4-ylamino)propan-2-yl)-2',3,5'-trifluoro-[1,1'-biphenyl]-4-carboxamide (27d)—The general procedure A was followed using **16d** to provide **27d** as a light yellow solid (70%). *R*_f = 0.42 (100% ethyl acetate). ¹H NMR (400 MHz, DMSO-*d*₆) δ 10.88 (d, *J* = 2.5 Hz, 1H), 10.64 (s, 1H), 8.61 (dd, *J* = 7.3, 3.3 Hz, 1H), 8.45 (d, *J* = 5.5 Hz, 2H), 7.73 – 7.65 (m, 2H), 7.63 – 7.58 (m, 2H), 7.57 – 7.47 (m, 3H), 7.42 (td, *J* = 9.5, 4.7 Hz, 1H), 7.37 – 7.29 (m, 2H), 7.25 (d, *J* = 2.4 Hz, 1H), 7.06 (ddd, *J* = 8.1, 6.9, 1.2 Hz, 1H), 6.97 (ddd, *J* = 8.0, 6.9, 1.0 Hz, 1H), 4.91 (td, *J* = 7.9, 5.5 Hz, 1H), 3.46 – 3.14 (m, 2H). ¹³C NMR (101 MHz, DMSO-*d*₆) δ 171.47, 163.26, 162.71, 160.45, 159.54, 157.97, 157.14, 156.42, 152.87, 150.62, 150.36, 145.48, 136.06, 130.54, 127.18, 123.93, 120.98, 118.48, 118.27, 117.12, 113.45, 111.34, 109.34, 55.13, 27.42. MS (ESI) 515 m/z [M + H]⁺.

(S)-N-(3-(1H-Indol-3-yl)-1-oxo-1-(pyridin-4-ylamino)propan-2-yl)-4'-chloro-3-fluoro-[1,1'-biphenyl]-4-carboxamide (27e)—The general procedure A was followed using **16e** to provide **27e** as a light yellow solid (60%). *R*_f = 0.32 (100% ethyl acetate). ¹H NMR (400 MHz, DMSO-*d*₆) δ 10.88 (d, *J* = 2.6 Hz, 1H), 10.65 (s, 1H), 8.51 (dd, *J* = 7.3, 3.9 Hz, 1H), 8.47 – 8.36 (m, 2H), 7.84 – 7.76 (m, 2H), 7.75 – 7.65 (m, 3H), 7.62 (ddd, *J* = 10.6, 5.3, 1.8 Hz, 3H), 7.58 – 7.52 (m, 2H), 7.33 (d, *J* = 8.1 Hz, 1H), 7.25 (d, *J* = 2.4 Hz, 1H), 7.06 (ddd, *J* = 8.1, 6.9, 1.2 Hz, 1H), 6.96 (ddd, *J* = 8.0, 7.0, 1.1 Hz, 1H), 4.91 (td, *J* = 8.0, 5.4 Hz, 1H), 3.45 – 3.15 (m, 2H). ¹³C NMR (101 MHz, DMSO-*d*₆) δ 171.50, 163.25, 161.12, 158.64, 154.72, 153.81, 150.35, 145.49, 136.58, 136.07, 133.57, 131.04, 129.04, 128.75, 127.19, 123.93, 122.46, 121.74, 120.99, 118.48, 118.27, 114.25, 114.01, 113.45, 111.35, 109.33, 55.12, 27.43. MS (ESI) 513 m/z [M + H]⁺.

(S)-N-(3-(1H-Indol-3-yl)-1-oxo-1-(pyridin-4-ylamino)propan-2-yl)-3'-chloro-3-fluoro-[1,1'-biphenyl]-4-carboxamide (27f)—The general procedure A was followed

using **16f** to provide **27f**, which was further purified by HPLC (36%, a white solid). ¹H NMR (400 MHz, DMSO-d₆) δ 10.88 (d, J = 2.5 Hz, 1H), 10.66 (s, 1H), 8.54 (dd, J = 7.3, 3.8 Hz, 1H), 8.49 – 8.39 (m, 2H), 7.85 (t, J = 1.9 Hz, 1H), 7.78 – 7.63 (m, 5H), 7.63 – 7.59 (m, 2H), 7.56 – 7.46 (m, 2H), 7.37 – 7.31 (m, 1H), 7.25 (d, J = 2.4 Hz, 1H), 7.06 (ddd, J = 8.1, 6.9, 1.2 Hz, 1H), 6.96 (ddd, J = 8.0, 7.0, 1.0 Hz, 1H), 4.92 (td, J = 7.9, 5.5 Hz, 1H), 3.44 – 3.15 (m, 2H). ¹³C NMR (101 MHz, DMSO-d₆) δ 171.50, 163.24, 161.07, 158.59, 150.28, 145.55, 143.03, 142.95, 139.89, 136.06, 133.93, 130.97, 130.89, 128.45, 127.18, 126.71, 125.67, 123.92, 122.69, 122.21, 122.07, 120.99, 118.48, 118.27, 114.55, 114.31, 113.45, 111.34, 109.34, 55.13, 27.43. MS (ESI) 513 *m/z* [M + H]⁺.

(S)-N-(3-(1H-Indol-3-yl)-1-oxo-1-(pyridin-4-ylamino)propan-2-yl)-2'-chloro-3-fluoro-[1,1'-biphenyl]-4-carboxamide (27g)—The general procedure A was followed using **16g** to provide **27g** as a white solid (80%). R_f = 0.51 (100% ethyl acetate). ¹H NMR (400 MHz, DMSO-d₆) δ 10.88 (d, J = 2.4 Hz, 1H), 10.65 (s, 1H), 8.62 (dd, J = 7.3, 3.2 Hz, 1H), 8.51 – 8.41 (m, 2H), 7.75 – 7.64 (m, 2H), 7.61 (dd, J = 4.8, 1.6 Hz, 4H), 7.49 – 7.43 (m, 3H), 7.38 (dd, J = 11.4, 1.6 Hz, 1H), 7.34 (dd, J = 7.9, 1.8 Hz, 2H), 7.26 (d, J = 2.4 Hz, 1H), 7.06 (ddd, J = 8.1, 6.9, 1.2 Hz, 1H), 6.97 (ddd, J = 8.0, 6.9, 1.0 Hz, 1H), 4.91 (td, J = 8.3, 5.6 Hz, 1H), 3.43 – 3.17 (m, 2H). ¹³C NMR (101 MHz, DMSO-d₆) δ 172.59, 171.53, 163.42, 160.13, 157.65, 155.83, 150.29, 145.55, 143.07, 137.78, 136.07, 131.62, 131.39, 131.11, 130.16, 130.03, 129.98, 127.67, 127.17, 125.44, 123.95, 122.42, 122.28, 120.99, 118.49, 118.26, 117.14, 116.90, 113.45, 111.34, 109.37, 55.15, 27.40. MS (ESI) 513.3 *m/z* [M + H]⁺.

(S)-N-(3-(1H-Indol-3-yl)-1-oxo-1-(pyridin-4-ylamino)propan-2-yl)-3,3',4'-trifluoro-[1,1'-biphenyl]-4-carboxamide (27h)—The general procedure A was followed using **16h** to provide **27h** as a white solid (78%). R_f = 0.45 (100% ethyl acetate). ¹H NMR (400 MHz, DMSO-d₆) δ 10.88 (d, J = 2.6 Hz, 1H), 10.65 (s, 1H), 8.53 (dd, J = 7.3, 3.8 Hz, 1H), 8.49 – 8.38 (m, 2H), 7.92 (ddd, J = 12.1, 7.7, 2.3 Hz, 1H), 7.75 – 7.49 (m, 8H), 7.33 (d, J = 8.0 Hz, 1H), 7.25 (d, J = 2.3 Hz, 1H), 7.06 (ddd, J = 8.1, 6.9, 1.2 Hz, 1H), 7.01 – 6.90 (m, 1H), 4.91 (td, J = 8.1, 5.6 Hz, 1H), 3.46 – 3.16 (m, 2H). ¹³C NMR (101 MHz, DMSO-d₆) δ 171.50, 163.22, 161.07, 158.59, 150.35, 145.49, 136.07, 130.97, 127.18, 123.93, 122.55, 122.08, 121.95, 120.99, 118.48, 118.27, 118.18, 118.00, 116.29, 116.11, 114.45, 114.21, 113.45, 111.35, 109.34, 55.14, 27.43. MS (ESI) 515.3 *m/z* [M + H]⁺.

(S)-N-(3-(1H-Indol-3-yl)-1-oxo-1-(pyridin-4-ylamino)propan-2-yl)-3,3'-difluoro-4'-methoxy-[1,1'-biphenyl]-4-carboxamide (27i)—The general procedure A was followed using **16i** to provide **27i**, which was further purified by HPLC (45%, a white solid). ¹H NMR (400 MHz, DMSO-d₆) δ 10.89 (d, J = 2.5 Hz, 1H), 10.81 (s, 1H), 8.48 (dd, J = 7.0, 4.2 Hz, 3H), 7.74 – 7.64 (m, 5H), 7.64 – 7.58 (m, 3H), 7.37 – 7.31 (m, 1H), 7.31 – 7.23 (m, 2H), 7.06 (ddd, J = 8.1, 6.9, 1.2 Hz, 1H), 6.96 (ddd, J = 8.0, 6.9, 1.0 Hz, 1H), 4.90 (td, J = 7.8, 5.6 Hz, 1H), 3.89 (s, 3H), 3.53 – 3.16 (m, 2H). ¹³C NMR (101 MHz, DMSO-d₆) δ 171.77, 163.31, 158.73, 152.96, 150.54, 149.03, 147.66, 147.56, 146.71, 136.07, 130.89, 127.16, 123.96, 123.22, 121.00, 118.45, 118.28, 114.27, 114.22, 113.74, 113.65, 113.51, 111.36, 109.25, 56.14, 55.21, 27.34. MS (ESI) 527.2 *m/z* [M + H]⁺.

(S)-N-(3-(1H-Indol-3-yl)-1-oxo-1-(pyridin-4-ylamino)propan-2-yl)-3'-cyano-3-fluoro-[1,1'-biphenyl]-4-carboxamide (27j)—The general procedure A was followed using **16j** to provide **27j** as a white solid (47%). ¹H NMR (400 MHz, DMSO-d₆) δ 10.89 (d, J = 2.5 Hz, 1H), 10.80 (s, 1H), 8.60 (dd, J = 7.4, 3.6 Hz, 1H), 8.48 (d, J = 5.6 Hz, 2H), 8.29 (t, J = 1.8 Hz, 1H), 8.12 (dt, J = 8.1, 1.3 Hz, 1H), 7.90 (dt, J = 7.8, 1.4 Hz, 1H), 7.80 – 7.74 (m, 1H), 7.74 – 7.64 (m, 6H), 7.33 (d, J = 8.1 Hz, 1H), 7.26 (d, J = 2.4 Hz, 1H), 7.11 – 7.02 (m, 1H), 6.96 (t, J = 7.3 Hz, 1H), 4.92 (td, J = 8.1, 5.6 Hz, 1H), 3.29 (dqt, J = 23.3, 14.6, 9.3,

8.5 Hz, 2H). ^{13}C NMR (101 MHz, DMSO- d_6) δ 171.68, 163.27, 161.08, 158.60, 149.34, 142.31, 138.83, 136.06, 132.14, 131.71, 131.03, 130.63, 130.27, 127.17, 123.95, 122.75, 120.99, 118.59, 118.47, 118.28, 114.70, 114.46, 113.60, 112.28, 111.35, 109.30, 55.23, 27.36. MS (ESI) 504 m/z [M + H] $^+$.

(S)-N-(3-(1H-Indol-3-yl)-1-oxo-1-(pyridin-4-ylamino)propan-2-yl)-4'-(benzyloxy)-3,3'-difluoro-[1,1'-biphenyl]-4-carboxamide (27k)—The general procedure A was followed using **16k** to provide **27k** as a light yellow solid (88%). R_f = 0.39 (100% ethyl acetate). ^1H NMR (400 MHz, DMSO- d_6) δ 10.90 (d, J = 2.5 Hz, 1H), 10.69 (s, 1H), 8.48 (dd, J = 7.4, 4.2 Hz, 1H), 7.87 – 7.52 (m, 8H), 7.51 – 7.38 (m, 5H), 7.38 – 7.30 (m, 4H), 7.25 (d, J = 2.4 Hz, 1H), 7.11 – 7.02 (m, 1H), 6.96 (t, J = 7.4 Hz, 1H), 5.26 (s, 2H), 4.91 (td, J = 8.0, 5.6 Hz, 1H), 3.40 – 3.16 (m, 2H). ^{13}C NMR (101 MHz, DMSO- d_6) δ 171.55, 163.25, 161.21, 158.73, 153.26, 150.84, 150.22, 146.62, 146.52, 145.55, 143.14, 143.06, 136.39, 136.07, 130.93, 130.90, 130.83, 130.78, 128.53, 128.11, 127.80, 127.19, 123.94, 123.17, 123.14, 122.00, 121.97, 121.19, 121.06, 120.99, 118.49, 118.27, 115.72, 114.67, 114.47, 113.78, 113.54, 111.35, 109.33, 70.24, 55.13, 29.60, 27.43. MS (ESI) 603 m/z [M + H] $^+$.

(S)-N-(3-(1H-Indol-3-yl)-1-oxo-1-(pyridin-4-ylamino)propan-2-yl)-3,3'-difluoro-4'-hydroxy-[1,1'-biphenyl]-4-carboxamide (27l)—The procedure for the synthesis of **3j** was followed using **27k** to provide **27l** as a brown solid (81%). ^1H NMR (400 MHz, DMSO- d_6) δ 10.88 (d, J = 2.5 Hz, 1H), 10.75 (s, 1H), 10.20 (s, 1H), 8.60 – 8.36 (m, 3H), 7.71 – 7.53 (m, 7H), 7.45 (dd, J = 8.4, 2.2 Hz, 1H), 7.33 (d, J = 8.1 Hz, 1H), 7.25 (d, J = 2.4 Hz, 1H), 7.10 – 7.00 (m, 2H), 6.96 (t, J = 7.4 Hz, 1H), 4.90 (td, J = 8.0, 5.6 Hz, 1H), 3.47 – 3.11 (m, 2H). ^{13}C NMR (101 MHz, DMSO- d_6) δ 171.70, 158.76, 149.42, 136.07, 127.16, 126.73, 123.95, 123.20, 121.74, 120.99, 118.46, 118.27, 111.36, 109.27, 55.17, 27.37. MS (ESI) 513 m/z [M + H] $^+$.

(S)-N-(3-(1H-Indol-3-yl)-1-oxo-1-(pyridin-4-ylamino)propan-2-yl)-4'-amino-3-fluoro-[1,1'-biphenyl]-4-carboxamide (27m)—The general procedure A was followed using **16l** to provide **27m** as a yellow solid (59%). ^1H NMR (400 MHz, DMSO- d_6) δ 10.88 (d, J = 2.5 Hz, 1H), 10.64 (s, 1H), 8.52 – 8.38 (m, 2H), 8.27 (dd, J = 7.2, 5.3 Hz, 1H), 7.64 (dd, J = 8.1, 6.2 Hz, 2H), 7.62 – 7.57 (m, 2H), 7.51 – 7.41 (m, 4H), 7.33 (d, J = 8.1 Hz, 1H), 7.24 (d, J = 2.4 Hz, 1H), 7.06 (ddd, J = 8.2, 6.9, 1.2 Hz, 1H), 6.99 – 6.92 (m, 1H), 6.64 (d, J = 8.6 Hz, 2H), 5.47 (s, 2H), 4.90 (td, J = 7.8, 5.5 Hz, 1H), 3.49 – 3.16 (m, 2H). ^{13}C NMR (101 MHz, DMSO- d_6) δ 171.58, 163.30, 161.48, 150.32, 149.68, 145.52, 136.08, 127.59, 127.19, 124.41, 123.93, 120.99, 120.66, 118.92, 118.79, 118.47, 118.27, 114.04, 113.44, 112.05, 111.81, 111.35, 109.29, 55.06, 27.45. MS (ESI) 494 m/z [M + H] $^+$.

(S)-N-(3-(1H-Indol-3-yl)-1-oxo-1-(pyridin-4-ylamino)propan-2-yl)-2-fluoro-4-(phenylethynyl)benzamide (27n)—The general procedure A was followed using **21b** to provide **27n** as a light yellow solid (86%). ^1H NMR (400 MHz, DMSO- d_6) δ 10.89 (d, J = 2.5 Hz, 1H), 10.68 (s, 1H), 8.66 (dd, J = 7.4, 3.1 Hz, 1H), 8.52 – 8.36 (m, 2H), 7.68 (d, J = 7.9 Hz, 1H), 7.65 – 7.56 (m, 5H), 7.52 (dd, J = 11.1, 1.5 Hz, 1H), 7.45 (dd, J = 7.0, 2.8 Hz, 4H), 7.34 (d, J = 8.1 Hz, 1H), 7.25 (d, J = 2.4 Hz, 1H), 7.07 (ddd, J = 8.1, 6.9, 1.2 Hz, 1H), 7.01 – 6.93 (m, 1H), 4.97 – 4.84 (m, 1H), 3.34 – 3.14 (m, 2H). ^{13}C NMR (101 MHz, DMSO- d_6) δ 171.45, 163.05, 160.32, 157.83, 150.39, 145.45, 136.07, 131.59, 130.76, 130.72, 129.43, 128.86, 127.54, 127.51, 127.17, 126.43, 126.33, 123.93, 123.38, 123.24, 121.50, 121.00, 118.90, 118.65, 118.50, 118.27, 113.44, 111.35, 109.34, 91.92, 87.54, 87.51, 55.15, 27.42. MS (ESI) 503.3 m/z [M + H] $^+$.

(S,E)-N-(3-(1H-Indol-3-yl)-1-oxo-1-(pyridin-4-ylamino)propan-2-yl)-4-(4-chlorostyryl)-2-fluorobenzamide (27o)—The general procedure A was followed using **17** to provide **27o** as a light yellow solid (78%). $R_f = 0.51$ (100% ethyl acetate). $^1\text{H NMR}$ (400 MHz, DMSO- d_6) δ 10.88 (d, $J = 2.5$ Hz, 1H), 10.67 (s, 1H), 8.55 – 8.33 (m, 3H), 7.72 – 7.57 (m, 6H), 7.54 (dd, $J = 12.4, 1.5$ Hz, 1H), 7.51 – 7.41 (m, 4H), 7.37 – 7.28 (m, 2H), 7.24 (d, $J = 2.4$ Hz, 1H), 7.06 (ddd, $J = 8.1, 7.0, 1.2$ Hz, 1H), 6.96 (ddd, $J = 8.0, 6.9, 1.0$ Hz, 1H), 4.90 (td, $J = 8.0, 5.6$ Hz, 1H), 3.44 – 3.12 (m, 2H). $^{13}\text{C NMR}$ (101 MHz, DMSO- d_6) δ 171.56, 163.23, 158.65, 150.17, 145.66, 141.97, 141.89, 136.07, 135.40, 132.67, 130.79, 130.31, 128.82, 128.50, 127.18, 123.94, 122.66, 121.32, 120.99, 118.48, 118.26, 113.46, 113.27, 111.35, 109.31, 55.13, 27.43. MS (ESI) 539.3 m/z $[\text{M} + \text{H}]^+$.

(S)-N-(3-(1H-Indol-3-yl)-1-oxo-1-(pyridin-4-ylamino)propan-2-yl)-2-fluoro-4-(phenylamino)benzamide (27p)—The general procedure A was followed using **20** to provide **27p** as a yellow solid (88%). $R_f = 0.33$ (100% ethyl acetate). $^1\text{H NMR}$ (400 MHz, DMSO- d_6) δ 10.89 (d, $J = 2.5$ Hz, 1H), 10.66 (s, 1H), 8.83 (s, 1H), 8.53 – 8.38 (m, 2H), 8.18 (s, 1H), 7.81 (t, $J = 7.4$ Hz, 1H), 7.70 – 7.54 (m, 3H), 7.42 – 7.27 (m, 3H), 7.22 (d, $J = 2.3$ Hz, 1H), 7.17 (d, $J = 7.8$ Hz, 2H), 7.03 (dt, $J = 19.1, 7.4$ Hz, 2H), 6.94 (t, $J = 7.4$ Hz, 1H), 6.85 (dd, $J = 8.7, 2.2$ Hz, 1H), 6.74 (dd, $J = 14.4, 2.2$ Hz, 1H), 4.96 – 4.80 (m, 1H), 3.27 (qd, $J = 14.7, 6.8$ Hz, 2H). $^{13}\text{C NMR}$ (101 MHz, DMSO- d_6) δ 171.74, 162.93, 162.90, 162.54, 160.09, 150.20, 148.88, 148.76, 145.65, 140.97, 136.11, 132.11, 132.07, 129.42, 127.19, 123.94, 122.23, 121.01, 119.48, 118.46, 118.28, 113.45, 111.37, 111.04, 110.92, 110.71, 109.20, 100.72, 100.44, 54.93, 27.56. MS (ESI) 494.2 m/z $[\text{M} + \text{H}]^+$.

(S)-N-(3-(1H-Indol-3-yl)-1-oxo-1-(pyridin-4-ylamino)propan-2-yl)-2-fluoro-4-morpholinobenzamide (27q)—The general procedure A was followed using **16m** to provide **27q** as a white solid (49%). $R_f = 0.48$ (10% MeOH in ethyl acetate), $R_f = 0.15$ (100% ethyl acetate). $^1\text{H NMR}$ (400 MHz, DMSO- d_6) δ 11.29 (s, 1H), 10.91 (d, $J = 2.5$ Hz, 1H), 8.68 – 8.49 (m, 2H), 7.96 – 7.78 (m, 3H), 7.70 – 7.53 (m, 2H), 7.32 (d, $J = 8.1$ Hz, 1H), 7.24 (d, $J = 2.4$ Hz, 1H), 7.04 (ddd, $J = 8.1, 6.9, 1.1$ Hz, 1H), 6.93 (ddd, $J = 8.0, 7.0, 1.0$ Hz, 1H), 6.86 – 6.69 (m, 2H), 4.88 (q, $J = 6.8$ Hz, 1H), 3.71 (dd, $J = 5.9, 3.9$ Hz, 4H), 3.44 – 3.18 (m, 6H). $^{13}\text{C NMR}$ (101 MHz, DMSO- d_6) δ 172.48, 136.08, 127.12, 124.03, 118.40, 118.29, 114.00, 111.37, 110.19, 109.53, 109.01, 65.71, 46.89, 45.87, 25.93. MS (ESI) 488.3 m/z $[\text{M} + \text{H}]^+$.

(S)-N-(3-(1H-Indol-3-yl)-1-oxo-1-(pyridin-4-ylamino)propan-2-yl)-2-fluoro-4-(4-(phenylsulfonyl)piperazin-1-yl)benzamide (27r)—The general procedure A was followed using **25b** to provide **27r** as a white solid (56%). $^1\text{H NMR}$ (400 MHz, DMSO- d_6) δ 10.85 (d, $J = 2.5$ Hz, 1H), 10.61 (s, 1H), 8.43 (d, $J = 5.5$ Hz, 2H), 7.85 – 7.70 (m, 4H), 7.70 – 7.62 (m, 2H), 7.62 – 7.51 (m, 4H), 7.31 (d, $J = 8.1$ Hz, 1H), 7.18 (d, $J = 2.4$ Hz, 1H), 7.04 (ddd, $J = 8.0, 7.0, 1.1$ Hz, 1H), 6.92 (ddd, $J = 8.0, 7.0, 1.1$ Hz, 1H), 6.79 – 6.67 (m, 2H), 4.92 – 4.79 (m, 1H), 3.39 (t, $J = 5.1$ Hz, 4H), 3.35 – 3.14 (m, 2H), 2.97 (t, $J = 5.0$ Hz, 4H). $^{13}\text{C NMR}$ (101 MHz, DMSO- d_6) δ 171.65, 162.87, 162.49, 160.03, 153.45, 150.22, 145.57, 136.06, 134.56, 133.45, 131.65, 131.60, 129.51, 127.58, 127.17, 123.89, 120.97, 118.41, 118.25, 113.42, 111.33, 110.86, 110.23, 109.18, 101.42, 54.91, 46.30, 45.34, 27.50. MS (ESI) 627 m/z $[\text{M} + \text{H}]^+$.

(S)-N-(3-(1H-Indol-3-yl)-1-oxo-1-(pyridin-4-ylamino)propan-2-yl)-2-fluoro-4-(piperazin-1-yl)benzamide hydrochloride (27s)—The general procedure A was followed using 4-(4-(*tert*-butoxycarbonyl)piperazin-1-yl)-2-fluorobenzoic acid obtained by hydrolysis of **23** (79%). $^1\text{H NMR}$ (400 MHz, CDCl_3) δ 9.37 (s, 1H), 8.60 (d, $J = 2.5$ Hz, 1H), 8.31 – 8.21 (m, 2H), 7.81 (t, $J = 9.1$ Hz, 1H), 7.56 (d, $J = 7.9$ Hz, 1H), 7.44 – 7.28 (m, 4H), 7.14 – 7.02 (m, 2H), 6.91 (t, $J = 7.5$ Hz, 1H), 6.61 (dd, $J = 9.1, 2.4$ Hz, 1H), 6.41 (dd, J

= 16.0, 2.4 Hz, 1H), 5.07 (q, J = 6.6, 6.1 Hz, 1H), 3.54 (dd, J = 6.8, 3.9 Hz, 4H), 3.41 – 3.33 (m, 2H), 3.25 (dd, J = 6.6, 4.1 Hz, 4H), 1.47 (s, 9H). The procedure for the synthesis of **3c** was followed to provide **27s**, which was further purified by HPLC (83%, a brown solid). ¹H NMR (400 MHz, DMSO-*d*₆) δ 12.43 (s, 1H), 11.03 (d, J = 2.5 Hz, 1H), 9.63 (s, 2H), 8.72 (d, J = 6.9 Hz, 2H), 8.34 – 8.18 (m, 2H), 8.02 (t, J = 6.8 Hz, 1H), 7.69 (d, J = 7.9 Hz, 1H), 7.61 (t, J = 8.9 Hz, 1H), 7.37 – 7.28 (m, 2H), 7.03 (t, J = 7.5 Hz, 1H), 6.90 (t, J = 7.6 Hz, 1H), 6.87 – 6.75 (m, 2H), 4.95 (dt, J = 8.2, 6.2 Hz, 1H), 3.56 (t, J = 5.1 Hz, 4H), 3.37 (qd, J = 14.6, 6.9 Hz, 2H), 3.15 (p, J = 4.3 Hz, 4H). ¹³C NMR (101 MHz, DMSO-*d*₆) δ 173.23, 163.08, 163.06, 162.64, 160.19, 153.49, 153.37, 153.11, 142.02, 136.12, 131.78, 131.74, 127.16, 124.23, 121.01, 118.58, 118.33, 114.57, 111.41, 111.01, 110.88, 110.27, 108.91, 101.64, 101.36, 55.80, 43.91, 42.01, 27.01. MS (ESI) 487.3 *m/z* [M + H]⁺.

(S)-N-(3-(1H-Indol-3-yl)-1-oxo-1-(pyridin-4-ylamino)propan-2-yl)-2-fluoro-4-(4-(4-fluorobenzyl)piperazin-1-yl)benzamide hydrochloride (27t)—The general procedure A was followed using **26b** to provide **27t**, which was further purified by HPLC (26%, a white solid). ¹H NMR (400 MHz, DMSO-*d*₆) δ 11.59 (s, 1H), 10.96 (d, J = 2.5 Hz, 1H), 8.69 (d, J = 6.8 Hz, 2H), 8.12 – 7.93 (m, 3H), 7.72 – 7.53 (m, 5H), 7.33 (ddd, J = 8.7, 6.3, 2.8 Hz, 3H), 7.26 (d, J = 2.4 Hz, 1H), 7.13 – 7.00 (m, 1H), 6.93 (t, J = 7.4 Hz, 1H), 6.90 – 6.77 (m, 2H), 4.87 (dt, J = 8.2, 6.0 Hz, 1H), 4.36 (s, 2H), 3.86 – 3.02 (m, 7H). ¹³C NMR (101 MHz, DMSO-*d*₆) δ 172.94, 163.99, 163.11, 161.54, 160.12, 158.53, 158.21, 153.03, 152.92, 151.54, 143.88, 136.11, 133.64, 133.55, 131.73, 127.08, 126.05, 124.13, 121.05, 118.34, 115.94, 115.72, 115.50, 114.39, 111.43, 111.26, 111.13, 110.33, 108.90, 101.72, 101.44, 57.87, 55.52, 49.87, 44.16, 27.04. MS (ESI) 595.4 *m/z* [M + H]⁺, 298.3 *m/z* [M + 2H]²⁺

General procedure B—synthesis of substituted biphenyl carboxylic acids

A mixture of 2-fluoro-4-bromobenzoic acid (**15**) (ca. 0.10 g, 0.46 mmol), phenyl boronic acid (ca. 1.1 eq), Pd₂(dba)₃ (3 mol%), PCy₃ (6 mol %), and K₃PO₄ (2 M, 1 mL) in dioxane (4 mL) was stirred under microwave heating (100 °C) for 1 h. The palladium catalyst was removed by filtration. The filtrate was acidified with 2N HCl (aq), and a white solid precipitated. The product mixture was diluted with ethyl acetate (30 mL) and washed with water (10 mL × 2) and brine (10 mL × 2). The organic layer was dried over magnesium sulfate, filtered, and concentrated in vacuo. The resulting product was purified by flash chromatography to afford 2-fluorobiphenylcarboxylic acid **16** in ca. 90% yield.

Hepatic microsomal stability

Microsome stability was evaluated by incubating 1 μM compound with 1 mg/mL hepatic microsomes (human, rat, or mouse) in 100 mM potassium phosphate buffer, pH 7.4 at 37 °C with continuous shaking. The reaction was initiated by adding NADPH, 1 mM final concentration. The final incubation volume was 300 μL and 40 μL aliquots were removed at 0, 5, 10, 20, 40, and 60 minutes. The aliquots were added to 160 μL acetonitrile to stop the reaction and precipitate the protein. NADPH dependence of the reaction is evaluated in parallel incubations without NADPH. At the end of the assay, the samples are centrifuged through a 0.45 micron filter plate (Millipore Solventer low binding hydrophilic plates, cat# MSRLN0450) and analyzed by LC-MS/MS. The data were log transformed and results are reported as half-life.

P450 inhibition

Cytochrome P450 inhibition was evaluated in human liver microsomes using four selective marker substrates (CYP1A2, phenacetin demethylation to acetaminophen; CYP2C9, tolbutamide hydroxylation to hydroxytolbutamide; CYP2D6, bufuralol hydroxylation to 4'-

hydroxybufuralol; and CYP3A4, midazolam hydroxylation to 1'-hydroxymidazolam) in the presence or absence of 10 or 1 μM test compound. The reaction is initiated by the addition of 1 mM NADPH and stopped after ten minutes by the addition of 2-times volume of acetonitrile containing dextrorphan as an internal standard. The concentration of each marker substrate is approximately its K_m .²¹ Furafylline, sulfaphenazole, quinidine, and ketoconazole were included in each run to validate that the assay could identify selective inhibitors of each isoform.

Molecular docking

The homology model of *Tc*CYP51 was generated based on the x-ray co-crystal structure of *Tb*CYP51 complexed with **14t** (PDB ID code: 4BJK) by using the homology model module implemented in Molecular Operating Environment (MOE). The homology model was refined with Protein Preparation Wizard implemented in Maestro 9.3. A receptor grid was generated from the refined structure using default values except for positional constraint at the nitrogen of 4-acylaminopyridine (radius: 0.8). The structure of **14t** was docked into the active site of *Tc*CYP51 by using Glide5.5 in extra precision (XP) mode with the predefined positional constraint (ligand feature: neutral acceptor). The binding pose of **14t** was the same as that in the original co-crystal structure with 1.5 Å RMSD of all atom pairs (maximum difference = 5.0 Å of fluoro atoms). The structures of **27k**, **27l**, **27r**, and **27s** were subsequently docked to the model structure of *Tc*CYP51 by applying the same parameters to predict their binding poses in the *Tc*CYP51 active site.

T. cruzi CYP51 expression, purification and UV-vis assay

Recombinant *Tc*CYP51 was expressed and purified as described elsewhere.^{18–19, 22} *Tc*CYP51 was used to monitor compound binding in UV-vis spectral assay as previously described.²² Binding affinity of hits was estimated from the titration curves using the quadratic tight-binding equation:²³

$$A_{\text{obs}} = (A_{\text{max}}/2E_t) \left\{ (S + E_t + K_D) - \left[(S + E_t + K_D)^2 - 4SE_t \right]^{0.5} \right\} \quad (1)$$

where A_{obs} is the absorption shift determined at any ligand concentration; A_{max} is the maximal absorption shift obtained at saturation; K_D is dissociation constant for the inhibitor-enzyme complex; S is the ligand concentration; E_t is the total enzyme concentration.

As differences in affinity between tight-binding ligands are reflected in the sharpness of the titration curve, K_D values recovered from fits to experimental data approximated by equation (1) are disproportionately sensitive to error in data points near inflection point, setting a limit to the method's sensitivity. Thus, caution was exercised when comparing the tight binding constants. At 0.5 μM *Tc*CYP51 working concentration, only the upper limit of K_D at 5 nM (a hundredth of the target concentration) could be estimated for the tightest binding inhibitors, if a plateau in the titration curve was reached at the stoichiometric enzyme-inhibitor ratio.

T. cruzi cell-based assay

EC_{50} of compounds were determined in the automated cell-based assay adapted from Engel and co-authors²⁴ and modified as previously described.²²

X-ray Crystallography

Recombinant *Tb*CYP51 mutant V34M/D249A/D250A/D251A modified by inserting a His₈-tag at the C-terminus and replacing the first 31 residues upstream of P32 with the fragment

MAKKTSSKGKL was used to obtain co-crystal structure with **14t**. Concentrated purified protein stored at -80°C was diluted to 0.1 mM prior to crystallization by mixing with water supplemented with **14t** to reach 1:1 protein:inhibitor ratio. Crystallization conditions were determined using commercial high-throughput screening kits available in deep-well format (Hampton Research), a nanoliter drop-setting Mosquito robot (TTP LabTech) operating with 96-well plates, and a hanging drop crystallization protocol. Crystals were further optimized in 96-well plates for diffraction data collection and harvested directly from the 200-nL drops. Prior to data collection, crystals were cryo-protected by plunging them into a drop of reservoir solution supplemented with 20% ethylene glycol, then flash frozen in liquid nitrogen.

Diffraction data were collected at 100–110 K at Beamline 8.3.1, Advanced Light Source, Lawrence Berkeley National Laboratory, USA. Data indexing, integration, and scaling were conducted using MOSFLM²⁵ and the programs implemented in the ELVES software suite.²⁶ The crystal structures were determined by molecular replacement using diffraction data processed in the C2 space group, with R_{merge} of 8.6% and atomic coordinates of *T. brucei* CYP51 (PDB ID code: 2×2N) as a search model. The final model was built using COOT²⁷ and refinement was performed by using REFMAC5 software²⁸ until R and R_{free} converged to 19.4% and 27.4%, respectively. Data collection and refinement statistics are shown in Table 5.

Only one of the four protein chains (chain A) constituting an asymmetric unit contained electron density corresponding to the whole molecule of **14t**; **14t** was assigned PDB code 18I. In three other chains, only the N-indolylpyridinyl portion of **14t** could be unambiguously placed. Thus, coordinates for the disordered biaryl moiety in chains B, C and D were omitted from the PDB entry.

Supplementary Material

Refer to Web version on PubMed Central for supplementary material.

Acknowledgments

We thank Mr. Potter Wickware for critical reading of the manuscript, the staff members of Beamline 8.3.1, James Holton, George Meigs and Jane Tanamachi, at the Advanced Light Source at Lawrence Berkeley National Laboratory, for assistance with data collection. This research was generously supported by NIH R01 grant AI095437, C.M.C was supported by Conselho Nacional de Desenvolvimento Científico e Tecnológico (CNPq) and FIOCRUZ, Brazil. The Advanced Light Source is supported by the Director, Office of Science, Office of Basic Energy Sciences, of the U.S. Department of Energy under Contract No. DE-AC02-05CH11231.

ABBREVIATIONS USED

<i>T. cruzi</i>	<i>Trypanosoma cruzi</i>
CYP51	cytochrome P450 family 51
CYP1A2, CYP2C9, CYP2D6, CYP3A4	cytochrome P450 isoform 1A2, 2C9, 2D6, and 3A4
SAR	structure activity relationship
SPR	structure property relationship
EC ₅₀	half maximal effective concentration

Reference

- (a) Bern C. Antitrypanosomal therapy for chronic Chagas' disease. *N. Engl. J. Med.* 2011; 364:2527–2534. [PubMed: 21714649] (b) Bern C, Kjos S, Yabsley MJ, Montgomery SP. *Trypanosoma cruzi* and Chagas' Disease in the United States. *Clin. Microbiol. Rev.* 2011; 24:655–681. [PubMed: 21976603] (c) Rassi A Jr, Rassi A, Marin-Neto JA. Chagas disease. *Lancet.* 2010; 375:1388–1402. [PubMed: 20399979] (d) Rossi MA, Tanowitz HB, Malvestio LM, Celes MR, Campos EC, Blefari V, Prado CM. Coronary microvascular disease in chronic Chagas cardiomyopathy including an overview on history, pathology, and other proposed pathogenic mechanisms. *PLoS Negl. Trop. Dis.* 2010; 4:e674. [PubMed: 20824217]
- Chagas C. Nova trypanozomíaze humana: estudos sobre a morfologia e o ciclo evolutivo do *Schizotrypanum cruzi* n. gen., n. sp., agente etiológico de nova entidade morbida do homem. *Mem. Inst. Oswaldo Cruz.* 1909; 1:159–218.
- (a) Apt W. Current and developing therapeutic agents in the treatment of Chagas disease. *Drug. Des. Devel. Ther.* 2010; 4:243–253. (b) Guedes PM, Silva GK, Gutierrez FR, Silva JS. Current status of Chagas disease chemotherapy. *Expert. Rev. Anti. Infect. Ther.* 2011; 9:609–620. [PubMed: 21609270]
- Rassi A Jr, Dias JC, Marin-Neto JA, Rassi A. Challenges and opportunities for primary, secondary, and tertiary prevention of Chagas' disease. *Heart.* 2009; 95:524–534. [PubMed: 19131444]
- (a) Buckner FS. Sterol 14-demethylase inhibitors for *Trypanosoma cruzi* infections. *Adv. Exp. Med. Biol.* 2008; 625:61–80. [PubMed: 18365659] (b) Lepesheva GI, Waterman MR. Sterol 14 α -demethylase (CYP51) as a therapeutic target for human trypanosomiasis and leishmaniasis. *Curr. Top. Med. Chem.* 2011; 11:2060–2071. [PubMed: 21619513]
- Kathiravan MK, Salake AB, Chothe AS, Dudhe PB, Watode RP, Mukta MS, Gadhwe S. The biology and chemistry of antifungal agents: a review. *Bioorg. Med. Chem.* 2012; 20:5678–5698. [PubMed: 22902032]
- (a) Lepesheva GI, Ott RD, Hargrove TY, Kleshchenko YY, Schuster I, Nes WD, Hill GC, Villalta F, Waterman MR. Sterol 14 α -demethylase as a potential target for antitrypanosomal therapy: enzyme inhibition and parasite cell growth. *Chem. Biol.* 2007; 14:1283–1293. [PubMed: 18022567] (b) Urbina JA, Payares G, Sanoja C, Molina J, Lira R, Brener Z, Romanha AJ. Parasitological cure of acute and chronic experimental Chagas disease using the longacting experimental triazole TAK-187. Activity against drug-resistant *Trypanosoma cruzi* strains. *Int. J. Antimicrob. Agents.* 2003; 21:39–48. [PubMed: 12507836]
- (a) Buckner FS, Urbina JA. Recent developments in sterol 14-demethylase inhibitors for Chagas Disease. *Int. J. Parasitol. Drugs Drug. Resist.* 2012; 2:236–242. [PubMed: 23277882] (b) Clayton J. Chagas disease: pushing through the pipeline. *Nature.* 2010; 465:S12–S15. [PubMed: 20571548]
- (a) Kraus JM, Tatipaka HB, McGuffin SA, Chennamaneni NK, Karimi M, Arif J, Verlinde CL, Buckner FS, Gelb MH. Second generation analogues of the cancer drug clinical candidate tipifarnib for anti-Chagas disease drug discovery. *J. Med. Chem.* 2010; 53:3887–3898. [PubMed: 20429511] (b) Kraus JM, Verlinde CL, Karimi M, Lepesheva GI, Gelb MH, Buckner FS. Rational modification of a candidate cancer drug for use against Chagas disease. *J. Med. Chem.* 2009; 52:1639–1647. [PubMed: 19239254]
- Andriani G, Amata E, Beatty J, Clements Z, Coffey BJ, Courtemanche G, Devine W, Erath J, Juda CE, Wawrzak Z, Wood JT, Lepesheva GI, Rodriguez A, Pollastri MP. Antitrypanosomal Lead Discovery: Identification of a Ligand-Efficient Inhibitor of *Trypanosoma cruzi* CYP51 and Parasite Growth. *J. Med. Chem.* 2013; 56:2556–2567. [PubMed: 23448316]
- (a) Chen CK, Leung SS, Guilbert C, Jacobson MP, McKerrow JH, Podust LM. Structural characterization of CYP51 from *Trypanosoma cruzi* and *Trypanosoma brucei* bound to the antifungal drugs posaconazole and fluconazole. *PLoS Negl. Trop. Dis.* 2010; 4:e651. [PubMed: 20386598] (b) Lepesheva GI, Hargrove TY, Anderson S, Kleshchenko Y, Furtak V, Wawrzak Z, Villalta F, Waterman MR. Structural insights into inhibition of sterol 14 α -demethylase in the human pathogen *Trypanosoma cruzi*. *J. Biochem.* 2010; 285:25582–25590.
- (a) Buckner FS, Wilson AJ, White TC, Van Voorhis WC. Induction of resistance to azole drugs in *Trypanosoma cruzi*. *Antimicrob. Agents Chemother.* 1998; 42:3245–3250. [PubMed: 9835521]

- (b) Kanafani ZA, Perfect JR. Antimicrobial resistance: resistance to antifungal agents: mechanisms and clinical impact. *Clin. Infect. Dis.* 2008; 46:120–128. [PubMed: 18171227]
13. (a) Chen CK, Doyle PS, Yermalitskaya LV, Mackey ZB, Ang KK, McKerrow JH, Podust LM. *Trypanosoma cruzi* CYP51 inhibitor derived from a *Mycobacterium tuberculosis* screen hit. *PLoS Negl. Trop. Dis.* 2009; 3:e372. [PubMed: 19190730] (b) Podust LM, von Kries JP, Eddine AN, Kim Y, Yermalitskaya LV, Kuehne R, Ouellet H, Warriar T, Altekoster M, Lee JS, Rademann J, Oschkinat H, Kaufmann SH, Waterman MR. Small-molecule scaffolds for CYP51 inhibitors identified by high-throughput screening and defined by X-ray crystallography. *Antimicrob. Agents Chemother.* 2007; 51:3915–3923. [PubMed: 17846131]
14. Doyle PS, Chen CK, Johnston JB, Hopkins SD, Leung SS, Jacobson MP, Engel JC, McKerrow JH, Podust LM. A nonazole CYP51 inhibitor cures Chagas' disease in a mouse model of acute infection. *Antimicrob. Agents Chemother.* 2010; 54:2480–2488. [PubMed: 20385875]
15. (a) Kumar S, Sharma R, Roychowdhury A. Modulation of cytochrome-P450 inhibition (CYP) in drug discovery: a medicinal chemistry perspective. *Curr. Med. Chem.* 2012; 19:3605–3621. [PubMed: 22680629] (b) Gubbins PO. Triazole antifungal agents drug-drug interactions involving hepatic cytochrome P450. *Expert Opin. Drug Metab. Toxicol.* 2011; 7:1411–1429. [PubMed: 21995615]
16. (a) Green M, Berman J. Preparation of pentafluorophenyl esters of Fmoc protected amino-acids with pentafluorophenyl trifluoroacetate. *Tetrahedron Lett.* 1990; 31:5851–5852. (b) Choi JY, Plummer MS, Starr J, Desbonnet CR, Soutter H, Chang J, Miller JR, Dillman K, Miller AA, Roush WR. Structure guided development of novel thymidine mimetics targeting *Pseudomonas aeruginosa* thymidylate kinase: from hit to lead generation. *J. Med. Chem.* 2012; 55:852–870. [PubMed: 22243413]
17. Ross D. The role of metabolism and specific metabolites in benzene-induced toxicity: evidence and issues. *J. Toxicol. Environ. Health A.* 2000; 61:357–372. [PubMed: 11086940]
18. Chen C-K, Doyle PS, Yermalitskaya LV, Mackey ZB, Ang KKH, McKerrow JH, Podust LM. *Trypanosoma cruzi* CYP51 inhibitor derived from a *Mycobacterium tuberculosis* screen hit. *PLoS Negl. Trop. Dis.* 2009; 3:e372. [PubMed: 19190730]
19. Chen C-K, Leung SSF, Guilbert C, Jacobson MP, McKerrow JH, Podust LM. Structural characterization of CYP51 from *Trypanosoma cruzi* and *Trypanosoma brucei* bound to the antifungal drugs posaconazole and fluconazole. *PLoS Negl. Trop. Dis.* 2010; 4:e651. [PubMed: 20386598]
20. Friesner RA, Murphy RB, Repasky MP, Frye LL, Greenwood JR, Halgren TA, Sanschagrin PC, Mainz DT. Extra precision glide: docking and scoring incorporating a model of hydrophobic enclosure for protein-ligand complexes. *J. Med. Chem.* 2006; 49:6177–6196. [PubMed: 17034125]
21. Testino SA Jr, Patonay G. High-throughput inhibition screening of major human cytochrome P450 enzymes using an in vitro cocktail and liquid chromatography-tandem mass spectrometry. *J. Pharm. Biomed. Anal.* 2003; 30:1459–1467. [PubMed: 12467917]
22. Gunatilleke SS, Calvet CM, Johnston JB, Chen CK, Erenburg G, Gut J, Engel JC, Ang KK, Mulvaney J, Chen S, Arkin MR, McKerrow JH, Podust LM. Diverse inhibitor chemotypes targeting *Trypanosoma cruzi* CYP51. *PLoS Negl. Trop. Dis.* 2012; 6:e1736. [PubMed: 22860142]
23. Morrison JF. Kinetics of the reversible inhibition of enzyme-catalysed reactions by tight-binding inhibitors. *Biochim. Biophys. Acta.* 1969; 185:269–286. [PubMed: 4980133]
24. Engel JC, Ang KKH, Chen S, Arkin MR, McKerrow JH, Doyle PS. Image-based high-throughput drug screening targeting the intracellular stage of *Trypanosoma cruzi*, the agent of Chagas' Disease. *Antimicrob. Agents Chemother.* 2010; 54:3326–3334. [PubMed: 20547819]
25. Leslie AGW. Recent changes to the MOSFLM package for processing film and image plate data. *Joint CCP4 ESF-EAMCB Newslett. Protein Crystallogr.* 1992:26.
26. Holton J, Alber T. Automated protein crystal structure determination using ELVES. *Proc. Natl. Acad. Sci. U S A.* 2004; 101:1537–1542. [PubMed: 14752198]
27. Emsley P, Cowtan K. Coot: model-building tools for molecular graphics. *Acta Crystallogr. D Biol. Crystallogr.* 2004; 60:2126–2132. [PubMed: 15572765]

28. (a) Murshudov GN, Vagin AA, Dodson EJ. Refinement of macromolecular structures by the maximum-likelihood method. *Acta Crystallogr. D Biol. Crystallogr.* 1997; 53:240–255. [PubMed: 15299926] (b) Collaborative Computational Project, Number 4. *Acta Crystallogr. D.* 1994; 50:760–763.
29. DeLano, WL. The PyMOL molecular graphics system. San Carlos, CA, USA: DeLano Scientific; 2002.
30. Pettersen EF, Goddard TD, Huang CC, Couch GS, Greenblatt DM, Meng EC, Ferrin TE. UCSF Chimera--a visualization system for exploratory research and analysis. *J. Comput. Chem.* 2004; 25:1605–1612. [PubMed: 15264254]

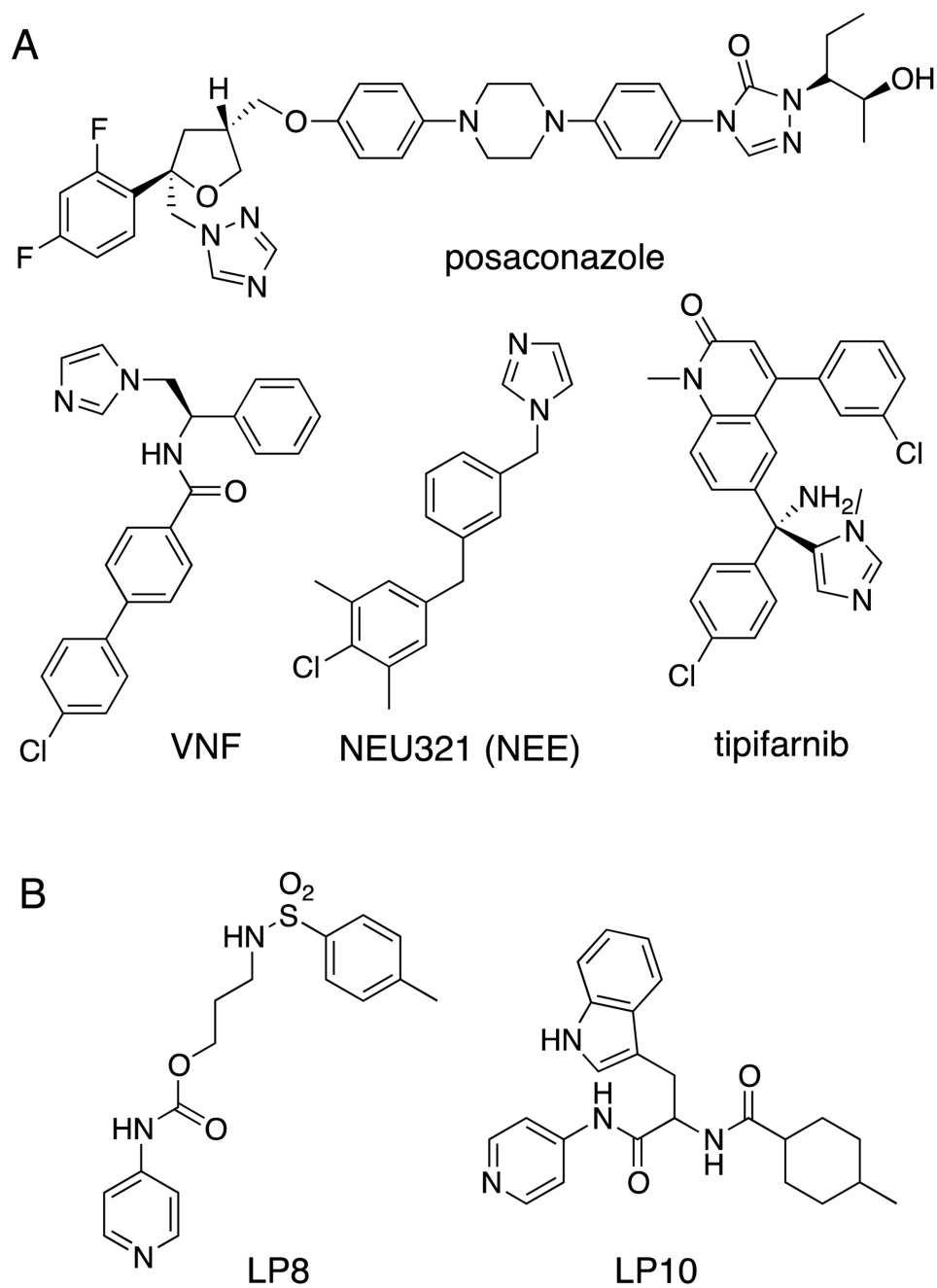


Figure 1. Inhibitors of *Tc*CYP51
(A) Azole type CYP51 inhibitors. (B) Pyridinyl type CYP51 inhibitors.

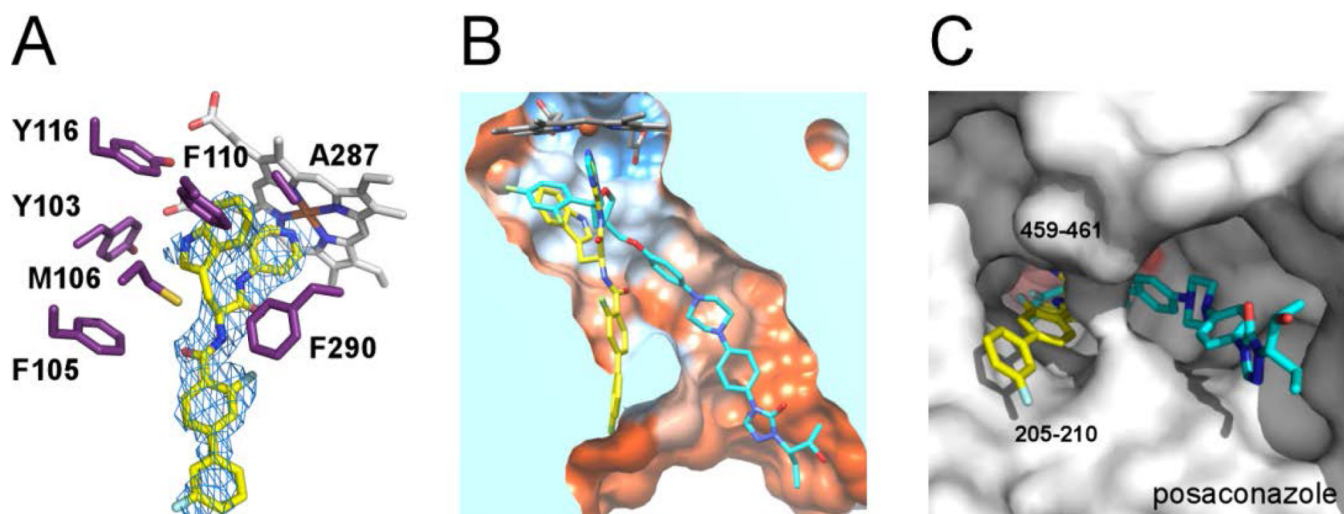


Figure 2. X-ray co-crystal structure of the *Tb* CYP51-14t complex

(A) Electron density map (blue mesh) contoured at 1.0σ delineates the positions of **14t** (yellow sticks) in the active site. In purple are amino acid residues providing hydrophobic contacts within 5 Å to the indol moiety of **14t** plus F105. Heme is displayed as grey sticks. (B) View of the **14t**-bound CYP51 clipped by a plane through the binding site compares the binding modes of **14t** (yellow) and posaconazole (cyan). The structure of *Tb*CYP51 complexed with posaconazole (PDB code: 2x2N) is superimposed on that of with **14t**. The active site surface is colored by hydrophobicity from orange (lipophilic) to blue (hydrophilic). (C) View of bound inhibitors from the entrance to the active site. The enzyme is represented by a gray surface. The hydrophobic units of posaconazole and **14t** occupy different hydrophobic tunnels in corresponding co-crystal structures. The images here and otherwise were generated using PYMOL²⁹ or CHIMERA³⁰.

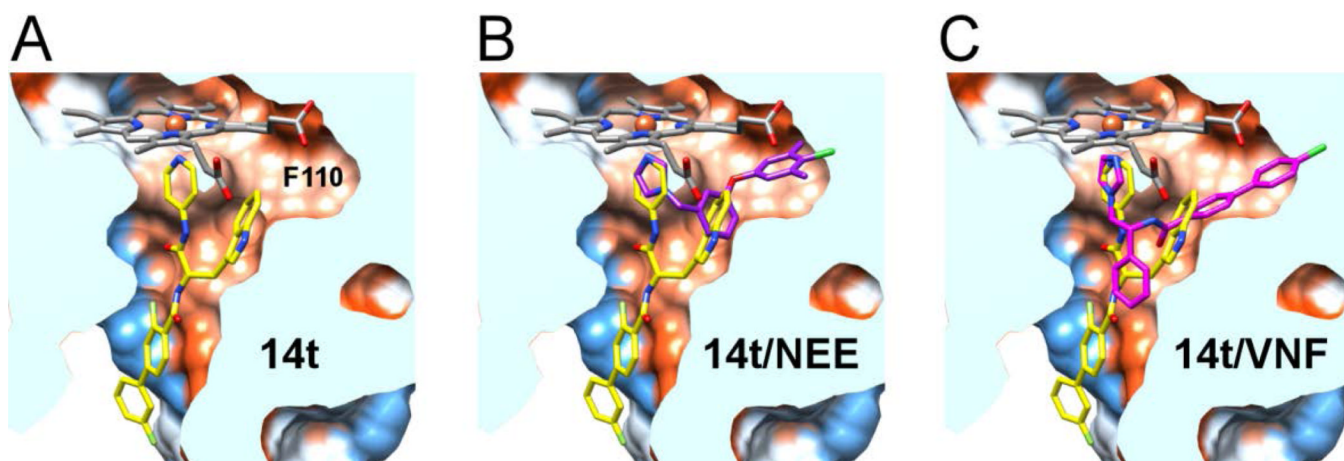


Figure 3. Comparison of the 14t binding mode with NEE and VNF

View of the **14t**-bound *TbCYP51* clipped by a plane through the binding site. A hydrophobic cavity accommodating the indole ring of **14t** (yellow) extends toward F110 (A). This extension accommodates a substituted benzyl ring in NEE (purple) (PDB ID 4H6O) (B) or biaryl moiety of VNF (pink) (PDB ID 3KSW) in the corresponding *TcCYP51* co-crystal structures. (C). Both structures were superimposed on the **14t**-bound *TbCYP51*.

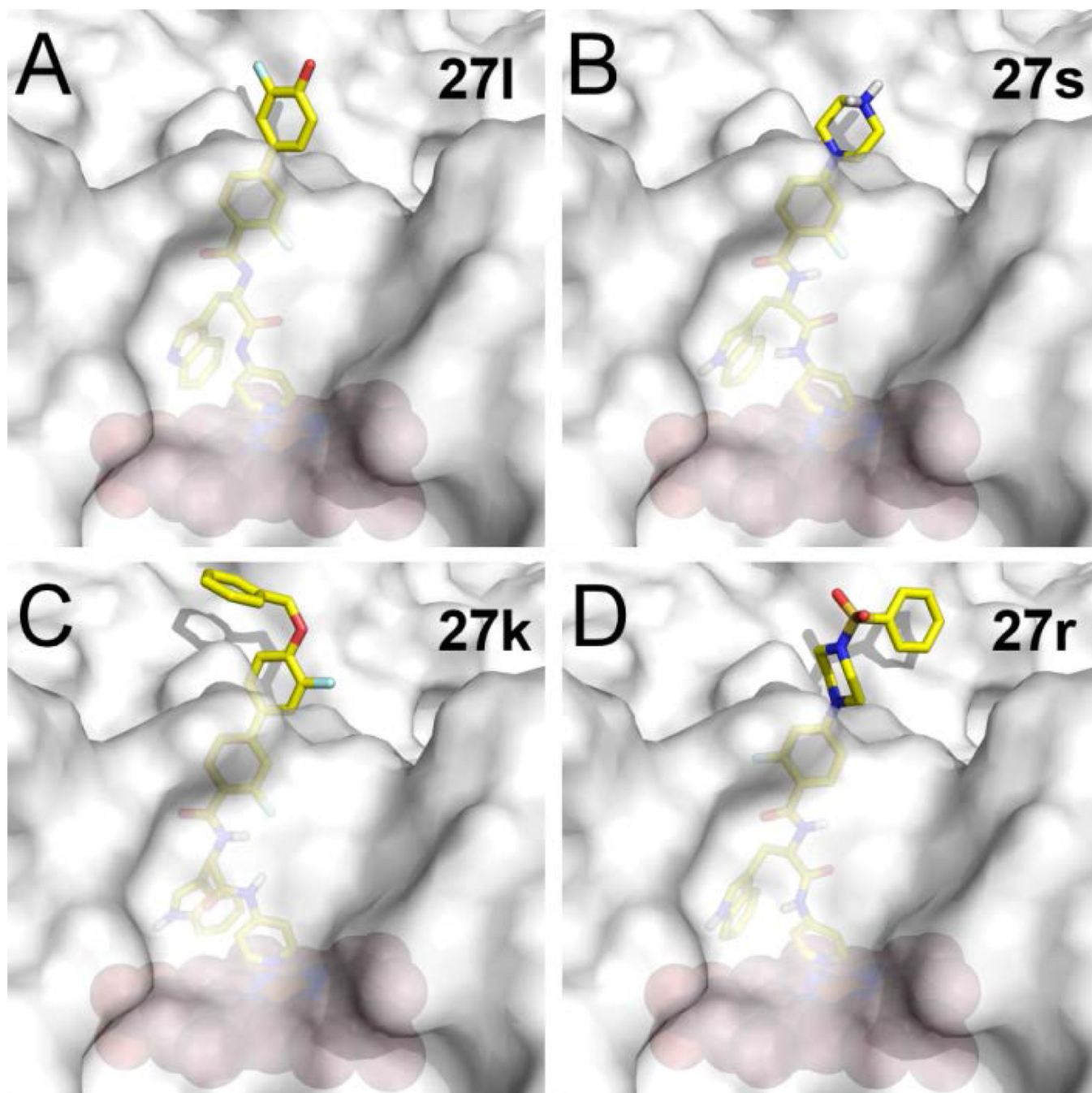
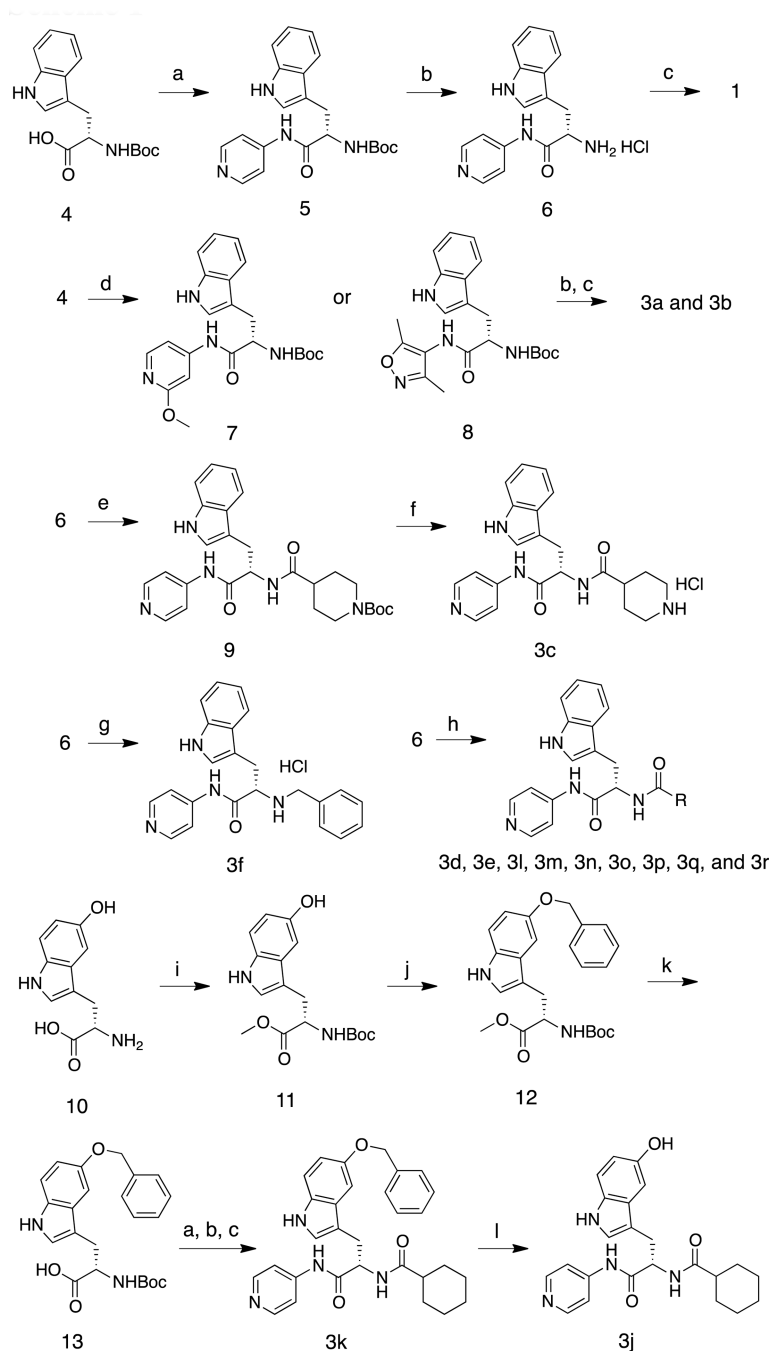


Figure 4. Predicted binding modes of inhibitors in *Tc* CYP51

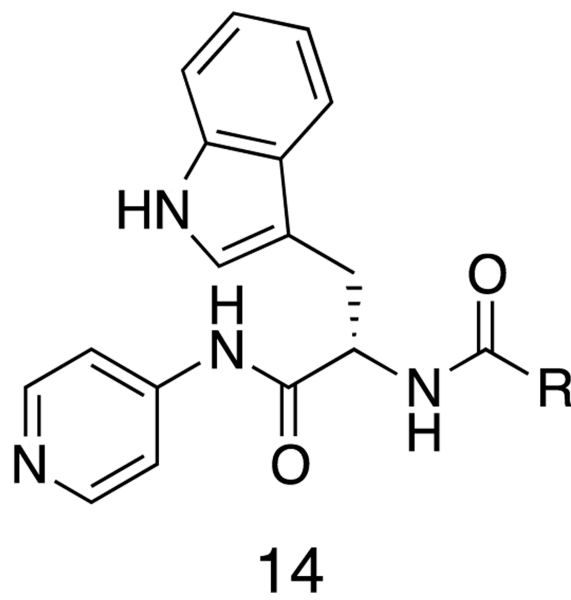
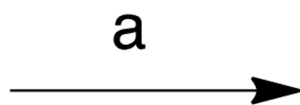
Binding modes of **27l** (A), **27s** (B), **27k** (C), and **27r** (D) resulting from molecular docking using Glide XP. Inhibitors are in stick mode colored by atom type: carbon in yellow, oxygen in red, nitrogen in blue, fluorine in cyan, hydrogen on the tertiary amino group of **27s** is in gray. The protein is shown as a semi-transparent gray surface; heme is displayed as orange spheres.

**Scheme 1.**

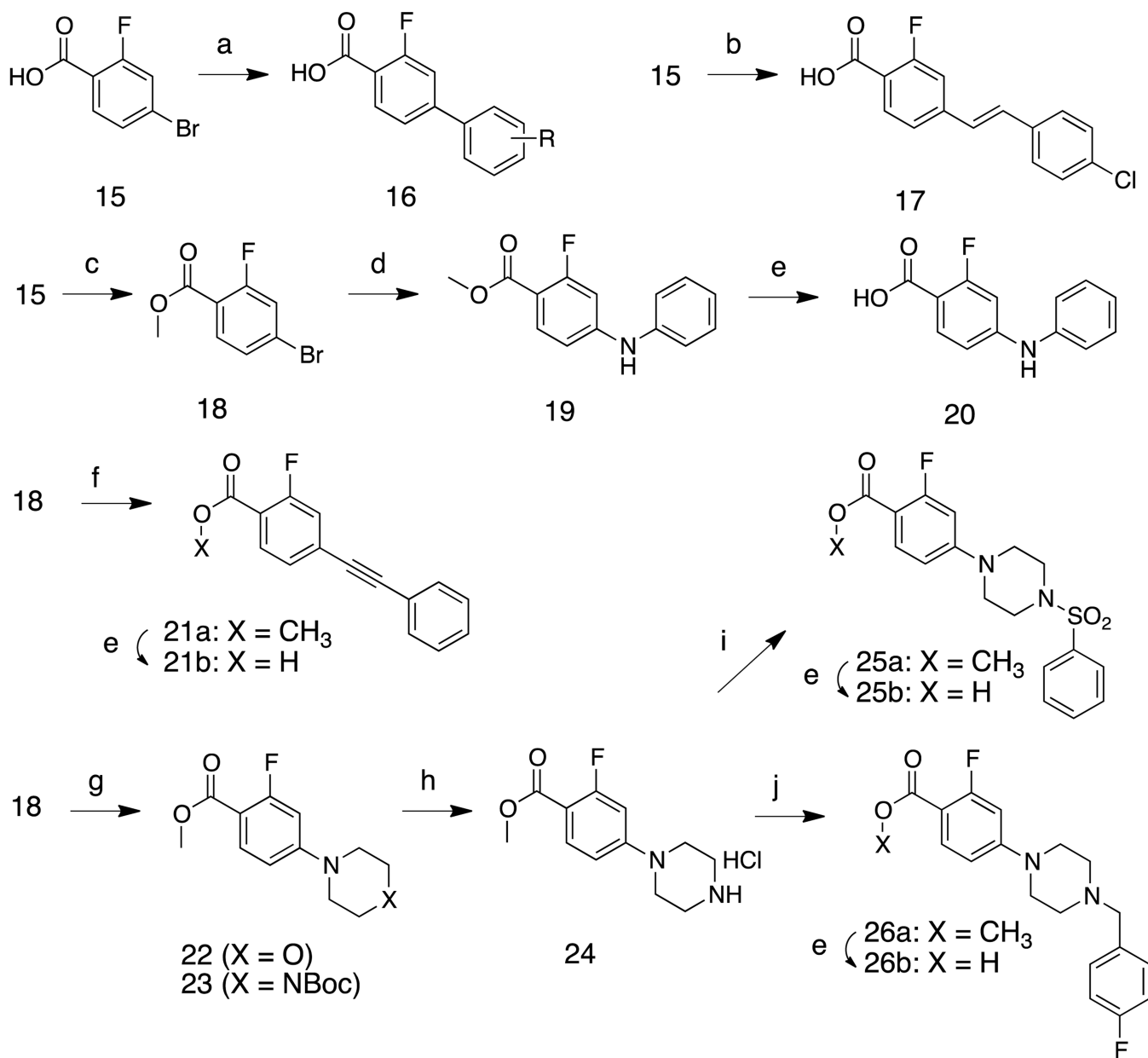
Reagents and conditions: (a) PyBOP, HOBt, NEt_3 , CH_2Cl_2 , 4-aminopyridine, 0 °C to room temp., 1h, 94%. (b) 4N HCl in dioxane, dioxane, room temp., 12h, >90% (crude) (c) cyclohexanecarbonyl chloride, NEt_3 , CH_2Cl_2 , 0 °C to room temp., 1h, 94%. (d) PyBOP, HOBt, NEt_3 , CH_2Cl_2 , 4-amino-2-methoxypyridine or 4-amino-3,5-dimethylisoxazole, 0 °C to room temp., 1h, 84%. (e) pentafluorophenyl trifluoroacetate, 1-Boc-tryptophan, NEt_3 , CH_2Cl_2 , 0 °C to room temp., 1h, 53%. (f) trifluoroacetic acid, CH_2Cl_2 , room temp., 1h, 47%. (g) benzylbromide, NEt_3 , CH_2Cl_2 , room temp., 12h, 30%. (h) pentafluorophenyl trifluoroacetate, NEt_3 , CH_2Cl_2 , alkyl carboxylic acids, 0 °C to room temperature, 1h, ~80%. (i) SOCl_2 , CH_3OH , 0 °C to room temp., 12h, then $(\text{Boc})_2\text{O}$, NEt_3 , CH_2Cl_2 , 0 °C to room

temp., 6h, 82%. (j) benzylbromide, Cs₂CO₃, acetone, room temp., 12h, 77%. (k) 10% NaOH, CH₃OH, 0 °C, 2h, 97%. (l) H₂, Pd/C, CH₃OH/THF, room temp., 24h, 29%.

6

**Scheme 2.**

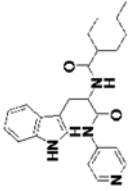
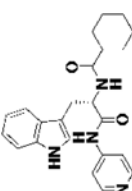
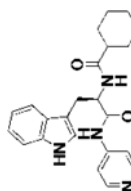
(a) PyBOP, HOBT, NEt₃, CH₂Cl₂, benzoic acids or naphthoic acids, 0 °C to room temp., 1h, typically 80%.

**Scheme 3.**

(a) Aryl boronic acid, 5 mol% Pd₂(dba)₃, 10 mol% PCy₃, 2M K₃PO₄, dioxane, 100 °C (microwave), 1h, ~90%. (b) 1-chloro-4-vinylbenzene, 5 mol% Pd(OAc)₂, 10 mol% P(o-tolyl)₃, Et₃N, DMF, 100 °C (microwave), 2h, 73%. (c) SOCl₂, CH₃OH, room temp. 12 h, 96%. (d) aniline, 5 mol% Pd(OAc)₂, 10 mol% BINAP, Cs₂CO₃, toluene, 100 °C (microwave), 2h, 73%. (e) 10% NaOH (aq), CH₃OH, 50 °C, 1h, 91%. (f) ethynylbenzene, 5 mol% Pd(OAc)₂, 10 mol% BINAP, Et₃N, CuI, toluene, 110 °C (microwave), 2h, 77%. (g) N-boc-piperazine or morpholine, Pd(OAc)₂, P(o-tolyl)₃, Cs₂CO₃, toluene, 50 °C, 48h, 91%. (h) trifluoroacetic acid, CH₂Cl₂, room temp. 1 h, >90% (crude). (i) phenylsulfonyl chloride, Et₃N, CH₂Cl₂, 0 °C to room temp. 1h, 81%. (j) 4-fluoro-benzyl bromide, Et₃N, CH₂Cl₂, room temp. 1h, 88%.

Table 1

Biochemical and cell-based activities, microsome stability and CYP inhibition properties of LP10 and analogs 1 and 2

compound	K_D (nM)	EC_{50} (μ M)	Microsome stability $t_{1/2}$ (min) ^a	% inhibition of human CYPs at 10 μ M (unless indicated otherwise)					
			h	m	1A2	2C9	2D6	3A4	
 LP10	42	0.65	-	-	-	-	-	-	
 1	5 ^c	0.68	3.8	4.2	41 (23) ^d	99 (92) ^d	93 (77) ^d	96 (75) ^d	
 2	140	1.5	6.5	6.9	55 (21) ^d	99 (92) ^d	96 (62) ^d	99 (77) ^d	
Sutent ^b	-	-	30	11	-	-	-	-	
Furafylline (40 μ M) ^b	-	-	-	-	86	5	4	8	
Sulfaphenazole ^b	-	-	-	-	20	92	7	21	
Quinidine ^b	-	-	-	-	23	9	90	36	
Ketoconazole (1 μ M) ^b	-	-	-	-	22	22	4	95	

^a Stability of compounds in human (h) and mouse (m) liver microsomes, using sunitinib as a reference control.

^b Reference compounds for microsome stability and human CYP inhibition

^c K_D of 5 nM (a hundredth of the target concentration) was estimated from the titration curves at 0.5 μ M 7cCYP51 for the tightest binding inhibitors, if a plateau was reached at the stoichiometric enzyme-inhibitor ratio.

^d Values in parentheses are % inhibition of the indicated human CYPs at 1 μ M.

Table 2

Biochemical and cell-based activities, microsome stability and CYP inhibition properties of inhibitors 3.^a

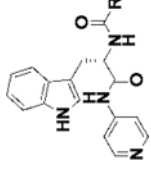
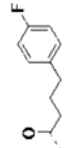
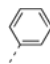
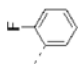
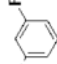
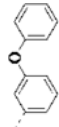
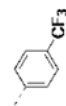
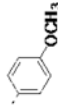
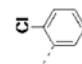
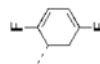
				K _D (nM)	EC ₅₀ (μM)	Microsome stability t _{1/2} (min)		%inhibition of human CYPs (at 10 μM)							
	R1	R2	R3			h	rat	m	1A2	2C9	2D6	3A4			
3a				n/b ^b	n/e ^c	5	2	2	25	16	30	50			
3b				n/b	n/e	4	4	2	24	39	5	22			
3c				n/b	n/e	>120	59	47	0	25	37	25			
3d				n/b	n/e	97	53	51	2	25	63	19			
3e				n/b	n/e	45	32	11	6	61	65	54			
3f				n/b	n/e	16	39	7	-26	13	69	23			
3g				<5	-	-	-	-	-	-	-	-			
3h				91	-	-	-	-	-	-	-	-			
3i				<5	3.0	3	3	2	22	96	91	96			

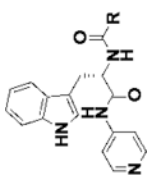
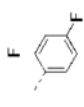
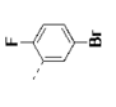
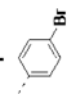
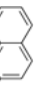
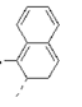
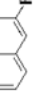
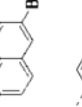
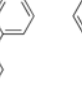
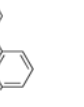
			K_D (nM)	EC_{50} (μ M)	Microsome stability $t_{1/2}$ (min)	%inhibition of human CYPs (at 10 μ M)					
3j			220	n/e	86	26	21	12	98	89	94
3k			<5	0.58	4	3	2	76	99	98	99
3l			792	3.2	6	7	5	14	98	86	94
3m			<5	0.90	5	3	2	26	99	93	98
3n			<5	0.61	6	3	2	44	98	91	99
3o			<5	0.30	4	3	3	64	99	96	97
3p			12	1.6	4	4	2	33	99	91	99
3q			14	0.85	3	3	3	54	99	96	99
3r			<5	0.16	6	3	3	51	96	84	86

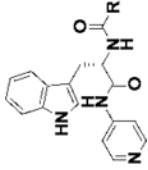
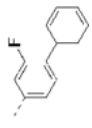
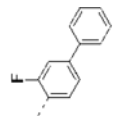
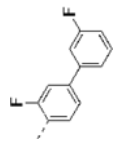
^aSee notes to Table 1^bn/b: no binding at 10 μ M^cn/e: not effective at 10 μ M

Table 3

Biochemical and cell-based activities, microsomal stability and CYP inhibition properties of inhibitors 14.^a

R		K_D (nM)	EC_{50} (μ M)	Microsome stability $t_{1/2}$ (min)		%inhibition of human CYPs (at 1 μ M, unless indicated otherwise)					
				h	Rat	m	1A2	2C9	2D6	3A4	
3r		<5	0.16	6	3	3	51 ^b	96 ^b	84 ^b	86 ^b	86 ^b
14a		<5	0.39	4	9	4	18 ^b	95 ^b	88 ^b	90 ^b	90 ^b
14b		<5	0.11	12	6	3	19 ^b	98 ^b	90 ^b	98 ^b	98 ^b
14c		<5	0.25	8	9	5	48 ^b	99 ^b	97 ^b	98 ^b	98 ^b
14d		<5	0.88	5	7	5	78 ^b	99 ^b	98 ^b	98 ^b	91 ^b
14e		<5	0.66	7	4	4	58 ^b	99 ^b	95 ^b	95 ^b	91 ^b
14f		38	0.35	8	8	6	46 ^b	99 ^b	92 ^b	92 ^b	92 ^b
14g		80	0.59	6	11	4	28 ^b	96 ^b	95 ^b	95 ^b	97 ^b
14h		95	0.21	6	9	3	29	86	64	80	80

		K_D (nM)	EC_{50} (μ M)	Microsome stability $t_{1/2}$ (min)	%inhibition of human CYPs (at 1 μ M, unless indicated otherwise)						
					32	42	89	59	94		
14i		<5	0.33	25	6	4	4	32	89	59	94
14j		60	0.036	9	8	4	4	42	94	86	90
14k		30	0.13	12	4	4	4	34	93	76	94
14l		<5	0.26	11	9	8	8	76 ^b	99 ^b	96 ^b	95 ^b
14m		<5	0.54	18	7	6	6	47	97	88	91
14n		<5	0.33	14	9	8	8	18	94	86	65
14o		50	0.46	29	23	18	18	41	95	73	77
14p		<5	0.55	19	19	23	23	67 ^b	99 ^b	95 ^b	92 ^b
14q		<5	0.89	10	6	5	5	80 ^b	99 ^b	98 ^b	92 ^b

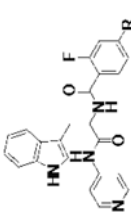
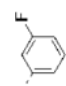
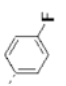
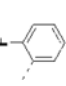
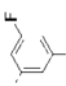
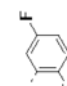
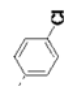
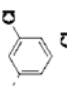
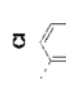
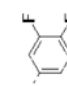
		K_D (nM)	EC_{50} (μ M)	Microsome stability $t_{1/2}$ (min)	%inhibition of human CYPs (at 1 μ M, unless indicated otherwise)					
14r		50	0.37	16	15	25	36	87	61	56
14s		<5	0.30	16	20	24	32	82	58	68
14t		<5	0.19	17	25	36	31	85	54	73

^a See notes to Table 1

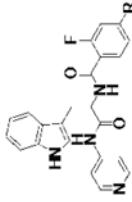
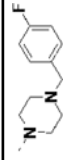
^b CYP inhibition for this compound was performed at 10 μ M

Table 4

Biochemical and cell-based activities, microsome stability and CYP inhibition properties of inhibitors 27.^a

		K_D nM	EC_{50} μ M	Microsome stability $t_{1/2}$ (min)		%inhibition of human CYPs (at 1 μ M, unless indicated otherwise)					
				h	Rat m	1A2	2C9	2D6	3A4		
14t		<5	0.19	17	25	36	31	85	54	73	
27a		<5	0.57	19	12	20	14	87	68	41	
27b		<5	0.28	18	13	23	14	85	58	63	
27c		<5	1.0	18	41	50	0	71	20	43	
27d		<5	0.28	12	15	22	3	77	34	58	
27e		<5	0.97	35	22	27	0	75	37	14	
27f		<5	0.98	21	36	53	10	80	34	41	
27g		<5	0.28	16	10	19	33	92	70	74	
27h		<5	0.97	22	20	32	48	93	75	54	

		K_D nM	EC_{50} μM	Microsome stability $t_{1/2}$ (min)	%inhibition of human CYPs (at 1 μM , unless indicated otherwise)					
27i		<5	0.014	23	14	10	91	38	69	
27j		<5	0.22	6	14	22	15	87	32	57
27k		<5	0.23	34	125	83	0	85	16	21
27l		<5	0.25	31	32	29	11	94	68	92
27m		<5	0.20	20	19	17	29	91	57	90
27n		<5	0.98	>120	67	104	23 (26) ^b	88 (96) ^b	28 (68) ^b	28 (46) ^b
27o		<5	0.98	70	67	53	21 (25) ^b	90 (94) ^b	63 (85) ^b	25 (33) ^b
27p		<5	0.47	28	31	25	12	94	83	79
27q		<5	0.057	13	19	7	10 (44) ^b	74 (98) ^b	66 (89) ^b	54 (94) ^b
27r		<5	0.018	7	19	3	37	97	85	61
27s		<5	0.46	15	36	41	5 (21) ^b	16 (71) ^b	22 (81) ^b	39 (82) ^b

		K_D nM	EC_{50} μ M	Microsome stability $t_{1/2}$ (min)	% inhibition of human CYPs (at 1 μ M, unless indicated otherwise)
27t		-	0.039	4 26 20	0 87 51 61

^a See notes to Table 1

^b Values in parentheses are % inhibition of the indicated human CYPs at 10 μ M

Table 5

Data collection and refinement statistics

Protein	<i>T. brucei</i> CYP51
Inhibitor	14t (Small molecule code 18I)
PDB ID	4BJK
Data collection	
Space group	C2
Cell dimensions	
<i>a, b, c</i> (Å)	199.3, 114.7, 136.22
α, β, γ (°)	90.0, 135.5, 90.0
Molecules in AU	4
Wavelength	1.11587
Resolution (Å)	2.67
R_{sym} or R_{merge} (%)	8.6 (88.8) ^d
$I / \sigma I$	7.7 (1.4)
Completeness (%)	99.9 (99.9)
Redundancy	4.1 (4.1)
Crystallization conditions	12% pentaerythritol propoxylate (5/4 PO/OH) 50 mM HEPES, pH 7.5 50 mM KCl 10% Jeffamine 600
Refinement	
No. reflections	60761
$R_{\text{work}} / R_{\text{free}}$ (%)	19.4/27.4
No. atoms	
Protein	14083
Heme	172
Ligand	100
Solvent	136
Mean B value	66.1
<i>B</i> -factors	
Protein	67.1
Heme	54.8
Ligand	84.9
Solvent	54.8
R.m.s deviations	
Bond lengths (Å)	0.011
Bond angles (°)	1.515

^dValues in parentheses are for highest-resolution.